Neurobiology of Disease

Disrupting the Balance of Protein Quality Control Protein UBQLN2 Accelerates Tau Proteinopathy

Julia E. Gerson,[1] Stephanie Sandoval-Pistorius,[1,2] Jacqueline P. Welday,[1] Aleija Rodriguez,[1] Jordan D. Gregory,[1] Nyjerus Liggans,[1] Kylie Schache,[1] Xingli Li,[1] Hanna Trzeciakiewicz,[1] Sami Barmada,[1] Lisa M. Sharkey,[1] and Henry L. Paulson[1]

[1]Department of Neurology, University of Michigan, Ann Arbor, Michigan 48109-5316, and [2]Neuroscience Graduate Program, University of Michigan, Ann Arbor, Michigan 48109-2215

Tau protein accumulation drives toxicity in several neurodegenerative disorders. To better understand the pathways regulating tau homeostasis in disease, we investigated the role of ubiquilins (UBQLNs)—a class of proteins linked to ubiquitin-mediated protein quality control (PQC) and various neurodegenerative diseases—in regulating tau. Cell-based assays identified UBQLN2 as the primary brain-expressed UBQLN to regulate tau. UBQLN2 efficiently lowered wild-type tau levels regardless of aggregation, suggesting that UBQLN2 interacts with and regulates tau protein under normal conditions or early in disease. Moreover, UBQLN2 itself proved to be prone to accumulation as insoluble protein in male and female tau transgenic mice and the human tauopathy progressive supranuclear palsy. Genetic manipulation of UBQLN2 in a tauopathy mouse model demonstrated that a physiological UBQLN2 balance is required for tau homeostasis. UBQLN2 overexpression exacerbated phosphorylated tau pathology and toxicity in mice expressing P301S mutant tau, whereas P301S mice lacking UBQLN2 showed significantly reduced phosphorylated tau. Further studies support the view that an imbalance of UBQLN2 perturbs ubiquitin-dependent PQC and autophagy. We conclude that changes in UBQLN2 levels, whether because of pathogenic mutations or secondary to disease states, such as tauopathy, contribute to proteostatic imbalances that exacerbate neurodegeneration.

Key words: **aggregation; autophagy; proteostasis; tau; ubiquitin proteasome system; UBQLN2**

Significance Statement

We defined a role for the protein quality control protein Ubiquilin-2 (UBQLN2), in age-related neurodegenerative tauopathies. This group of disorders is characterized by the accumulation of tau protein aggregates, which differ when UBQLN2 levels are altered. Given the lack of effective disease-modifying therapies for tauopathies and the function of UBQLN2 in handling various disease-linked proteins, we explored the role of UBQLN2 in regulating tau. We found that UBQLN2 reduced tau levels in cell models but behaved differently in mouse brain, where it accelerated mutant tau pathology and tau-mediated toxicity. A better understanding of the diverse functions of regulatory proteins like UBQLN2 can elucidate some of the causative factors in neurodegenerative disease and outline new routes to therapeutic intervention.

Introduction

Tau is a natively unstructured protein cleared by different protein degradation pathways depending on its folding and aggregation state, post-translational modifications, mutations, and other factors altering its conformation. In its native state, tau can be degraded by the proteasome in a ubiquitin-independent manner (Jones et al., 2017), while ubiquitin-dependent proteasomal clearance is likely more important in disease states and is impaired in both Alzheimer's disease (AD) and tauopathy models (Keller et al., 2000; Cripps et al., 2006; Myeku et al., 2016). These observations suggest that ubiquitin-dependent proteasomal clearance counters disease and may normally regulate tau. Further studies suggest that ubiquitin–proteasome system clearance of misprocessed tau is facilitated by molecular chaperones

Received May 27, 2021; revised Dec. 9, 2021; accepted Dec. 21, 2021.

Author contributions: J.E.G., H.T., S.B., L.M.S., and H.L.P. designed research; J.E.G., S.S.-P., J.P.W., A.R., J.D.G., N.L., K.S., X.L., and H.T. performed research; S.B. contributed unpublished reagents/analytic tools; J.E.G., S.S.-P., J.P.W., A.R., J.D.G., N.L., and K.S. analyzed data; J.E.G. wrote the paper.

The authors declare no competing financial interests.

This work was supported by National Institutes of Health Grants 9R01-NS-096785-06, 1P30-AG-053760-01, F32-AG-059362-01, and T32-NS-007222-36; the Alzheimer's Association; and The Amyotrophic Lateral Sclerosis Foundation. We thank Peter Howley and Huda Zoghbi for providing constructs; Rakez Kayed for providing mouse tissue; the Michigan Brain Bank for providing human disease tissue; Nick Kanaan and Peter Davies for providing antibodies; Venkatesha Basrur and the Mass Spectrometry Facility of the Department of Pathology at the University of Michigan for mass spectrometry analysis; and Paulson laboratory members for helpful suggestions.

Correspondence should be addressed to Henry L. Paulson at henryp@med.umich.edu.

https://doi.org/10.1523/JNEUROSCI.1116-21.2021

(Shimura et al., 2004). While activation of macroautophagy reduces levels of mutant tau aggregates (Schaeffer et al., 2012), chaperone-mediated autophagy (CMA) inefficiently clears mutant or aberrantly post-translationally modified tau, despite wild-type tau being a substrate for CMA (Caballero et al., 2018, 2021).

Tau homeostasis likely depends on a balance of proteostatic regulators. The protein clearance factor Ubiquilin-2 (UBQLN2) has been implicated in numerous neurodegenerative diseases (Mori et al., 2012). Further study of UBQLN2 may offer insight into the dysregulation of tau protein quality control (PQC) in disease. UBQLN2 is one member of a family of brain-expressed UBQLN proteins that also include UBQLN1 and UBQLN4. All UBQLNs possess N-terminal ubiquitin-like and C-terminal ubiquitin-associated domains. The functional presence of both domains enables UBQLNs to shuttle ubiquitinated proteins to the proteasome for degradation (Elsasser et al., 2002; Rao and Sastry, 2002). Though principally implicated in proteasomal clearance of ubiquitinated substrates, UBQLN2 may also modulate autophagic clearance of aggregates (Chuang et al., 2016).

The discovery of missense mutations in UBQLN2 that directly cause frontotemporal dementia (FTD) and amyotrophic lateral sclerosis (ALS; Deng et al., 2011; Williams et al., 2012; Fahed et al., 2014; Scotter et al., 2017) underscored the importance of UBQLN2 in neurodegenerative proteinopathies. In contrast, weaker evidence indirectly links another UBQLN, UBQLN1, to neurodegenerative disease (Bertram et al., 2005; Brouwers et al., 2006; Slifer et al., 2006; Smemo et al., 2006). We and others have shown that UBQLN1 and UBQLN2 both colocalize with polyglutamine aggregates in Huntington's disease (Doi et al., 2004; Safren et al., 2015; Zeng et al., 2015; Hjerpe et al., 2016) and with amyloid deposits in AD and FTD (Deng et al., 2011; Mizukami et al., 2014). A genetic variant of a third UBQLN, UBQLN4, is also associated with familial FTD (Edens et al., 2017).

Recent studies support a broader role for UBQLN2 in common neurodegenerative diseases. For example, phosphorylated α-synuclein deposits are associated with UBQLN2 in Parkinson's disease (PD) and dementia with Lewy bodies brains (Mori et al., 2012; Rutherford et al., 2013). With respect to tauopathies, less is known about the relationship between UBQLN2 and tau, but lower levels of soluble UBQLN2 in AD brain suggest dysregulation of UBQLN2 in tauopathies (Nölle et al., 2013). In addition to sequestering other aggregating proteins, UBQLN2 itself is prone to aggregate and undergo liquid–liquid phase separation (LLPS) *in vitro* (Hjerpe et al., 2016; Dao et al., 2018; Sharkey et al., 2018). While both UBQLN1 and UBQLN4 share the ability to undergo LLPS with UBQLN2, the three UBQLN proteins diverge in liquid droplet characteristics and aggregation behavior, implying that, despite their similarity, functional differences may exist (Gerson et al., 2021).

There is a need to further understand the dual role of UBQLN2 in regulating protein clearance on the one hand, and its potential to induce toxicity through the formation of aggregates or stabilization of aggregation-prone protein substrates on the other hand. While data link UBQLN2 to advanced fibrillar pathology of other amyloidogenic proteins (Mori et al., 2012; Rutherford et al., 2013), it is unknown whether UBQLN2 regulates tau under normal conditions or in disease states. Moreover, why three different UBQLN proteins are expressed in the brain remains an open question. Using cellular models, transgenic (Tg) mouse models and human disease tissue, we now report a previously unrecognized role for UBQLN2 in regulating tau toxicity.

Materials and Methods

Plasmids and siRNAs

The pCMV4-FLAG-UBQLN2 plasmid (p4455 FLAG-hPLIC-2; plasmid #8661, Addgene) and pCS2-FLAG-UBQLN1 plasmid (p4458 FLAG-hPLIC-1; plasmid #8663, Addgene) were gifts from Peter Howley (Harvard Medical School, Boston MA). UBQLN1 was cloned into the pCMV4 vector. UBQLN4 was cloned from pDONR223-UBQLN4 (pENTR-A1UP; plasmid #16170, Addgene), which was a gift from Huda Zoghbi (Baylor College of Medicine, Houston, TX), into the pCMV4-FLAG vector. The pCMV4-FLAG-UBQLN1+PXX plasmid was synthesized by VectorBuilder. Wild-type 0N4R tau [microtubule-associated protein tau (MAPT)] was cloned from pEGFP-tau into the pCMV vector. Control empty vector plasmid for cell transfection experiments was pCMV-HA. Dharmacon SMARTpool siGENOME siRNA against UBQLN1, UBQLN2, and UBQLN4 and MISSION siRNA Universal Negative Control (Sigma-Aldrich) were used for UBQLN1, UBQLN2, and UBQLN4 knock-down experiments. The pCMV-wild-type 0N4R tau-Dendra2 plasmid was synthesized by VectorBuilder. Creation of the pGW1-UBQLN2-iRFP and pGW1-iRFP plasmids is described in the study by Sharkey et al. (2018).

Cell transfection

Human embryonic kidney 293 (HEK293) cells were cultured in high-glucose DMEM, supplemented with 10% FBS, 10 mM glutamine, and 100 U/ml penicillin/streptomycin. Cells were transfected with pCMV4-FLAG-UBQLN1, pCMV4-FLAG-UBQLN2, pCMV4-FLAG-UBQLN4, pCMV4-FLAG-UBQLN1+PXX, UBQLN1 siRNA, UBQLN2 siRNA, UBQLN4 siRNA, or empty vector/control siRNA in combination with pCMV-tau using Lipofectamine 2000 according to the manufacturer instructions. Cortical primary neurons were dissected from rat pups at embryonic day 20. Neurons were plated on laminin/poly-D-lysine-coated 96-well plates (Archbold et al., 2018; Malik et al., 2018; Flores et al., 2019; Safren et al., 2021) at a density of 1×10^5 cells/well in NEUMO photostable media supplemented with SOS (Cell Guidance Systems). Neurons were transfected with plasmids encoding tau-Dendra2 and UBQLN2-iRFP or iRFP using Lipofectamine 2000 as before (Archbold et al., 2018; Malik et al., 2018; Flores et al., 2019; Safren et al., 2021).

Optical pulse labeling

Imaging of primary neurons was accomplished using an inverted microscope (Eclipse Ti, Nikon) equipped with Semrock filter sets, Sutter λ 421 multi-LED light source, and an Andor Zyla 4.2(+) sCMOS camera (Oxford Instruments), enclosed in a custom-built environmental chamber to maintain a temperature of 37°C and 5% CO_2 levels. All stage movements, filter switching, illumination, and image acquisition were controlled through μManager with original code written in BeanShell, as described previously. Image processing and analyses were accomplished through dedicated software written expressly for these purposes (Malik et al., 2018; Weskamp et al., 2019). Fluorescence was initially measured 24 h following transfection. We then used a 3 s pulse of 405 nm light for Dendra2 photoconversion, and obtained images again 3 h following photoconversion and then every 24 h for the following 3 d, as previously described (Barmada et al., 2014; Malik et al., 2018; Flores et al., 2019). Only cells that survived the entire duration of the experiment were included for further analysis. The half-life of tau-Dendra2 in individual neurons was determined by fitting the time-dependent decline in photoconverted (red) tau-Dendra2 fluorescence for each cell to a first-order exponential decay curve.

Human disease brain tissue

Frozen brain tissue from the mid-frontal cortex was obtained from progressive supranuclear palsy (PSP) and age-matched control subjects (Table 1) from the Michigan Brain Bank (University of Michigan, Ann Arbor, MI). Brain tissue was collected with patient consent, and protocols were approved by the Institutional Review Board of the University of Michigan and abide by the Declaration of Helsinki principles. Samples were examined at autopsy by neuropathologists for pathologic diagnosis with the indicated postmortem intervals (PMI).

Table 1. Tauopathy samples used for UBQLN2 analysis

Tauopathy tissue			
Diagnosis	Sex	Age (years)	PMI (h)
Control	Female	74	6
Control	Female	76	14
Control	Male	65	14
Control	Male	83	28
PSP	Female	54	12
PSP	Female	66	12
PSP	Female	78	6
PSP	Female	79	6
PSP	Female	88	15
PSP	Male	64	4
PSP	Male	66	5
PSP	Male	73	3
PSP	Male	73	4
PSP	Male	73	4
PSP	Male	77	12
PSP	Male	79	6

PMI, Postmortem interval.

Mouse models

This study was conducted in a facility approved by the American Association for the Accreditation of Laboratory Animal Care, and all experiments were performed in accordance with the National Institutes of Health *Guide for the Care and Use of Laboratory Animals* and approved by the Institutional Animal Care and Use Committee of the University of Michigan. Mice were housed at the University of Michigan animal care facility and maintained according to US Department of Agriculture standards (12 h light/dark cycle with food and water available *ad libitum*). Twelve-month-old hemizygous UBQLN2-high (Hi) transgenic mice generated in the laboratory (Sharkey et al., 2018, 2020), and Non-Tg littermates were killed with isoflurane and perfused with PBS, and brains were removed for analysis. Additionally, we acquired brains from 6-, 9-, and 18-month-old human tau (Htau) mice [B6.Cg-*Mapt*$^{tm1(EGFP)Klt}$ Tg-MAPT 8cPdav/J; stock #005491, The Jackson Laboratory (courtesy of Rakez Kayed, University of Texas Medical Branch, Galveston, TX); Andorfer et al., 2003] and 3-, 6-, 8-, and 11-month-old P301S tau mice (B6;C3-Tg-Prnp-MAPT-P301S PS19Vle/J; stock #008169, The Jackson Laboratory; Yoshiyama et al., 2007) and nontransgenic littermates.

Hemizygous UBQLN2-Hi and UBQLN2-Low transgenic mice were crossed to hemizygous P301S mice. In addition, male homozygous UBQLN2 knock-out (KO) mice (Sharkey et al., 2020) were crossed to hemizygous P301S mice to produce P301S males homozygous for UBQLN2 knockout and P301S females hemizygous for UBQLN2 knockout. The resulting mice were used for breeding to yield both male and female P301S mice homozygous for UBQLN2 knockout. Because UBQLN2-high and UBQLN2 knock-out mice are on the same genetic background, nontransgenic littermates from F1 generations of both breeding schemes were used as controls. At 3, 6, and 9 months of age, nontransgenic littermates, UBQLN2-high transgenic, UBQLN2 knockout, P301S, P301SxUBQLN2-high transgenic, and P301SxUBQLN2 knock-out mice were killed with isoflurane and perfused with PBS, and brains were removed for analysis. Nontransgenic littermates, UBQLN2-low transgenic, P301S, and P301SxUBQLN2-low transgenic mice were killed at 9 months for brain collection. Brains were dissected and divided sagittally. one half (of the brain) was immediately placed on dry ice and stored at −80°C for biochemical studies, while the other half was fixed in 4% paraformaldehyde at 4°C for 24 h and cryoprotected in a series of 10–30% sucrose in 0.1 M phosphate buffer at 4°C until saturated. Fixed hemispheres were sectioned at 12 μm sagittally using a cryostat. Sections were stored at −20°C for immunohistochemistry studies. For paraffin sections, hemi-brains were fixed in 4% paraformaldehyde at 4°C for 48 h and stored in 70% ethanol before paraffin embedding and sectioning at 5 μm sagittally conducted by Zyagen. Both male and female mice were included in analyses.

Open field

Using mice assigned to both 9 and 6 month brain collection timepoints, we evaluated locomotor activity at 6 months of age (3 d before the collection date for 6 month cohorts) in mouse crosses using the open-field task. Each mouse was placed in the center of a circular, white, open-field arena (height, 42 cm; diameter, 44.5 cm; Chem-Trainer) and allowed to freely explore for 2 min before testing. Afterward, exploratory behavior of each mouse was recorded for 15 min with a CCD camera controlled by Limelight software (Actimetrics).

Novel object recognition

On the day immediately following the open-field task, mice were placed in the same open-field arena for the training phase of novel object recognition, adapted to differentiate objects based on texture from previously described methods (Wu et al., 2013) because of visual deficits associated with UBQLN2 overexpression (Sharkey et al., 2020). Two identical cubes were placed in the open-field arena and held in place with adhesive tack, and mice were allowed to explore for 15 min. On the third day, mice were placed again in the arena for 15 min with one familiar object previously explored in the training phase and one novel object sharing a common size, shape, color, and volume but differing in texture. After each trial, the apparatus was thoroughly cleaned using 70% ethanol and allowed to dry before placement of a new mouse. Trials were recorded and the time spent exploring each object was measured using Limelight software (Actimetrics). Exploration was defined by head orientation within 2 cm of the object or physical contact with the object. The percentage of total time spent exploring the familiar object versus the novel object was measured. To control for any differences in exploratory behavior, the discrimination index was also calculated as the time spent exploring the familiar object subtracted from the time spent exploring the novel object, divided by the total time spent exploring both objects. Object exploration data were analyzed using GraphPad Prism version 5.04 software by one-way ANOVA and Tukey's *post hoc* test.

UBQLN2 immunoprecipitation from brain lysates

Mouse brain samples used for tau immunoprecipitation (IP) were homogenized in RIPA buffer supplemented with protease inhibitor cocktail (catalog #11873580001, Sigma-Aldrich), Halt phosphatase inhibitor cocktail (Thermo Fisher Scientific) and deacetylase inhibitors, 10 mM nicotinamide, and 2 μM Trichostatin A using a 1:3 dilution of tissue/RIPA (w/v). Samples were centrifuged at 16,000 relative centrifugal force for 30 min at 4°C. Supernatants from both spins were combined. Brain lysates were precleared before immunoprecipitation using a mixture of Protein A and G beads (New England Biolabs). Cleared lysate was incubated overnight at 4°C with rotation in anti-FLAG, clone M2 (Sigma-Aldrich). The next day, a mixture of Protein A and G beads was incubated with the lysate–antibody mixture overnight at 4°C with rotation. UBQLN2 protein was eluted in 3× SDS + DTT and boiled for 5 min at 70°C immediately before loading on precast NuPAGE 4–12% Bis-Tris gels (Thermo Fisher Scientific).

Western blot analysis

Cells used for Western blot analyses of total protein lysate were lysed in 1× RIPA buffer supplemented with protease inhibitor cocktail, then water sonicated for 5 min and centrifuged for 30 min at 16,000 rcf at 4°C. Following BCA (Thermo Fisher Scientific) quantification, cell lysates containing 10 μg of total protein or equal volumes of immunoprecipitate were loaded on precast NuPAGE 4–12% Bis-Tris gels (Thermo Fisher Scientific) for SDS-PAGE analysis. Gels were subsequently transferred onto nitrocellulose membranes (0.45 μm) and either stained with Ponceau-S for total protein quantification and destained or immediately blocked for 1 h at room temperature with 10% nonfat dry milk in 1× TBS-T buffer. Membranes were then probed overnight at 4°C in anti-Ubiquilin-2 (1:2000; Novus Biologicals), anti-FLAG, clone M2 (1:1000; Sigma-Aldrich), anti-Tau, clone Tau5 (1:5000; BioLegend), anti-Ubiquilin-1 (1:2000; Novus Biologicals), anti-A1UP (UBQLN4; 1:2000; Santa Cruz Biotechnology) or anti-GAPDH (1:5000; Millipore) diluted in 5% nonfat dry milk. HRP-conjugated goat anti-rabbit IgG or goat

anti-mouse IgG (1:5000) was used for detection as appropriate. ECL (Thermo Fisher Scientific) was used to visualize bands, which were normalized to corresponding GAPDH or Ponceau levels. All quantification of immunoblots was performed by densitometric analysis using ImageJ software (National Institutes of Health). Analyses were completed in triplicate and analyzed by one-way ANOVA with the Tukey's *post hoc* test.

Soluble and insoluble mouse and human brain samples were homogenized using the Bullet Blender (Next Advance) in 1× PBS supplemented with protease inhibitor cocktail (catalog #11873580001, Sigma-Aldrich), using a 1:3 dilution of tissue/PBS (w/v). Samples were centrifuged at 10,000 rcf for 10 min at 4°C. Supernatants (PBS-soluble fraction) were aliquoted, snap frozen, and stored at −80°C until use. For insoluble fractions, pellets were resuspended in 1× PBS supplemented with protease inhibitor cocktail and centrifuged at 10,000 rcf for 10 min at 4°C, and supernatants were discarded. The remaining pellet was resuspended in 1% Sarkosyl in 1× PBS supplemented with protease inhibitor, vortexed for 1 min, and incubated at room temperature for 1 h. Samples were water sonicated for 5 min and centrifuged for 20 min at 16,000 rcf at 4°C. Supernatants were discarded, and the procedure was repeated with remaining pellet for insoluble fraction. Following BCA (Thermo Fisher Scientific) quantification, brain extracts containing 25 μg of total protein in LDS sample buffer (catalog #NP0007, Thermo Fisher Scientific) were loaded (without boiling) on precast NuPAGE 4–12% Bis-Tris gels (Thermo Fisher Scientific) for SDS-PAGE analysis. For total brain lysates, mouse brain samples were homogenized in 1× RIPA buffer with protease inhibitor cocktail (catalog #11873580001, Sigma-Aldrich), using a 1:3 dilution of tissue/RIPA (w/v). Samples were centrifuged at 16,000 rcf for 30 min at 4°C. Supernatants were aliquoted, snap frozen, and stored at −80°C until use. Brain extracts containing 25 μg of total protein were loaded after boiling on precast NuPAGE 4–12% Bis-Tris gels (Thermo Fisher Scientific) for SDS-PAGE analysis.

Western blots were conducted as described above and probed in anti-Ubiquilin-2 (1:2000; Novus Biologicals), anti-Tau, clone Tau5 (1:5000; BioLegend), anti-Ubiquilin-1 (1:2000; Novus Biologicals), anti-A1UP (UBQLN4; 1:2000; Santa Cruz Biotechnology), anti-human tau, clone HT7 (1:2000; Thermo Fisher Scientific), anti-phosphorylated tau (1:2000; pT231, AT180; Thermo Fisher Scientific), anti-phosphorylated tau (pS202, pT205, AT8; 1:1000; Thermo Fisher Scientific), anti-phosphorylated tau (pS396; 1:20,000; Abcam), anti-phosphorylated tau (pS202; 1:2000; Cell Signaling Technology), anti-LAMP2A (1:1000; Abcam), anti-LC3A (1:5000; Novus Biologicals), anti-p62 (1:1000; MBL International), anti-polyubiquitinated conjugates (FK1; 1:1000; Enzo), anti-ubiquitin (1:3000; Millipore), anti-Hsp70-72 (1:5000; Enzo), anti-Hsp90β (1:1000; Enzo), anti-FKBP5 (1:2000; ABclonal), anti-GSK3β (1:1000; Cell Signaling Technology) anti-pGSK3β (1:2000; Cell Signaling Technology), anti-α-tubulin (1:1000; Cell Signaling Technology), or anti-GAPDH (1:10,000; Millipore) diluted in 5% nonfat dry milk. HRP-conjugated goat anti-rabbit IgG, goat anti-mouse IgG, goat anti-mouse IgM, or goat anti-guinea pig IgG (1:5000) was used for detection as appropriate. EcoBright Nano HRP Western blot substrate (Innovative Solutions) was used to visualize bands, which were normalized to corresponding α-tubulin, GAPDH, or Ponceau total protein levels, using the Syngene G:Box imaging system. All quantification of immunoblots was performed by densitometric analysis using ImageJ software (National Institutes of Health). Analyses were completed in triplicate and analyzed by one-way ANOVA with the Tukey's *post hoc* test, the Kruskal–Wallis test, two-way ANOVA, linear regression or the Student's *t* test as appropriate.

RNA isolation and quantitative real-time PCR

RNA from transiently transfected HEK293 cells expressing empty vector alone, tau and empty vector/control siRNA, tau and UBQLN2, or tau and UBQLN2 siRNA was obtained using the RNeasy Mini Kit (Qiagen) following the manufacturer instructions. Reverse transcription of 500 ng of total RNA per sample was performed using the iScript cDNA Synthesis Kit (BIO-RAD). Tau and GAPDH (housekeeping) transcript levels were assessed by quantitative real-time PCR (qRT-PCR). Relative gene expression was determined using the CT method, normalizing for GAPDH mRNA levels. Results are displayed as fold change relative to GAPDH over endogenous levels of tau in empty vector alone cells.

The following primers were used: Tau 441 qPCR, forward, 5′-CGCCAGGAGTTCGAA-3′; Tau 441 qPCR, reverse, 5′-GGCCAG GGAGGCAGA-3′; GAPDH qPCR forward, 5′-AGATCCCTCCAAA ATCAAGTGG-3′; and GAPDH qPCR reverse, 5′-GGCAGAGATG ATGACCCTTTT-3′.

Immunofluorescence

Cells analyzed by immunofluorescence were fixed in chilled methanol for 15 min at −20°C. Fixed cells were washed in 1× PBS, permeabilized with 0.5% Triton X-100, and blocked in 5% goat serum for 1 h. Cells were incubated in anti-Ubiquilin-2 (1:200; Novus Biologicals) or anti-Ubiquilin-1 (1:100; Novus Biologicals) and anti-Tau, Tau5 (1:100; BioLegend) overnight at 4°C. The following day, cells were washed in PBS three times for 10 min each and incubated with goat anti-rabbit IgG Alexa Fluor-568 (1:500; Thermo Fisher Scientific) and goat anti-mouse IgG Alexa Fluor-488 (1:500; Thermo Fisher Scientific) for 1 h. Cells were then washed in PBS three times for 10 min each and incubated with DAPI (Sigma-Aldrich) to label nuclei for 5 min at room temperature, washed three times for 5 min each, and mounted with Prolong Gold Antifade Reagent (Thermo Fisher Scientific). Slides were imaged using an inverted microscope (model IX71, Olympus) and analyzed for tau fluorescence using the Cell Counter tool in ImageJ.

Brain sections were postfixed in chilled methanol, subjected to heated antigen retrieval in 10 mM citrate buffer, pH 6, permeabilized with 0.5% Triton X-100 and blocked using the M.O.M. Immunodetection Kit (Vector Laboratories) according to manufacturer instructions. Sections were incubated in anti-Ubiquilin-2 (1:250; Novus Biologicals), anti-tau, Tau5 (1:150; BioLegend), anti-phosphorylated tau, AT8 (1:200), anti-phosphorylated tau pS202/pT205 (1:500; Stressmarq), anti-p62 (1:200), anti-polyubiquitinated conjugates, FK1 (1:200; Enzo), or anti-LAMP2A (5 μg/ml) overnight at 4°C. The following day, sections were washed in PBS three times for 10 min each and incubated for 1 h with goat anti-rabbit IgG, goat anti-mouse IgG, goat-anti-guinea pig IgG, or goat anti-mouse IgM Alexa Fluor-594/405/488/647 (1:500; Thermo Fisher Scientific) as appropriate. Sections were then washed in PBS three times for 10 min each and—other than in cases where triple staining was completed—sections were incubated with DAPI (Sigma-Aldrich) to label nuclei for 5 min at room temperature, washed three times for 5 min each, and coverslipped with Prolong Gold Antifade Reagent (Thermo Fisher Scientific). Slides were imaged with a Leica SP5 confocal microscope and analyzed for corrected total cell fluorescence in ImageJ (National Institutes of Health) as previously described (Burgess et al., 2010), using the Analyze Particles tool in ImageJ to determine the total number of puncta per cell or field or the EZColocalization tool in ImageJ as previously described (Stauffer et al., 2018).

Thioflavin S staining

Paraffin sections from Non-Tg, P301S, and P301SxUBQLN2-high mice were heated, deparaffinized, and rehydrated with sequential dilutions of xylene, ethanol, and distilled water. Sections were incubated in 70% ethanol for 5 min and then incubated in autofluorescence eliminator reagent (Sigma-Aldrich) for 5 min and washed in three changes of 70% ethanol. Sections were then incubated in 1% filtered Thioflavin S in 80% ethanol for 15 min at room temperature protected from light. Sections were sequentially washed in 80−70% ethanol and distilled water, then coverslipped using Prolong Gold Antifade Reagent (Thermo Fisher Scientific). Sections colabeled with UBQLN2 were subjected to heated antigen retrieval in 10 mM citrate buffer, pH 6, and permeabilized with 0.5% Triton X-100 after deparaffinization and rehydration. Sections were incubated in 70% ethanol for 5 min and then incubated in autofluorescence eliminator reagent (Sigma-Aldrich) for 5 min and washed in three changes of 70% ethanol. Afterward, sections were blocked in 5% goat serum for an hour at room temperature and incubated in anti-Ubiquilin-2 (1:250; Novus Biologicals) overnight at 4°C. The following day, sections were washed in PBS three times for 10 min each and incubated for 1 h with goat anti-rabbit IgG 647 (1:500; Thermo Fisher Scientific). Sections were then washed in PBS three times for 10 min each and then incubated in Thioflavin S and washed as described above.

Slides were imaged with a Leica SP5 confocal microscope using a 405 nm wavelength absorbance and quantified for number of tangles using the Analyze Particles tool in ImageJ.

Dot blot analysis

PBS-soluble brain lysates containing 5 μg of total protein in 1 μl were directly spotted onto nitrocellulose membranes and allowed to dry for 1 h. Loading control membranes were stained with Ponceau-S for total protein quantification. Dot blot membranes were blocked for 1 h at room temperature with 10% nonfat dry milk in TBS-T buffer and then probed overnight at 4°C in anti-misfolded tau antibody Alz50 (1:2000; a gift from Peter Davies (Albert Einstein College of Medicine; New York)) diluted in 5% nonfat dry milk. HRP-conjugated goat anti-mouse IgM (1:5000) was used for detection. EcoBright Nano HRP Western blot substrate (Innovative Solutions) was used to visualize dots using the Syngene G:Box imaging system, which were normalized to corresponding Ponceau stain. All quantification was performed by densitometric analysis using ImageJ software. Analyses were completed in triplicate and analyzed by one-way ANOVA with the Tukey's *post hoc* test.

LC Tandem mass spectrometry

Sample preparation. Mouse brain samples used for tau immunoprecipitation were homogenized in RIPA buffer supplemented with protease inhibitor cocktail (catalog #11873580001, Sigma-Aldrich), Halt phosphatase inhibitor cocktail (Thermo Fisher Scientific), and deacetylase inhibitors, 10 mM nicotinamide, and 2 μM Trichostatin A using a 1:3 dilution of tissue/RIPA (w/v). Samples were centrifuged at 16,000 rcf for 30 min at 4°C. Supernatants were removed and pellet was resuspended in RIPA homogenization buffer and centrifuged again at 16,000 rcf for 30 min at 4°C. Supernatants from both spins were combined. Brain lysates were precleared before immunoprecipitation using a mixture of Protein A and G beads (New England Biolabs). Cleared lysate was incubated overnight at 4°C with rotation in a mixture of anti-tau antibodies, Tau13 (Abcam), rabbit polyclonal tau antibody (Abcam), and Tau-5 (BioLegend). The next day, a mixture of Protein A and G beads was incubated with the lysate–antibody mixture overnight at 4°C with rotation. Tau protein was eluted in 3× SDS + DTT and boiled for 5 min at 70°C immediately before loading on precast NuPAGE 4–12% Bis-Tris gels (Thermo Fisher Scientific). The gel containing 80% of the IP sample was labeled with SimplyBlue Safe Stain (Thermo Fisher Scientific). A second gel containing 20% of the IP samples was used for downstream Western blot characterization of IP samples.

In-gel digestion. Protein samples were processed and analyzed at the Mass Spectrometry Facility of the Department of Pathology at the University of Michigan. Two gel slices corresponding to endogenous and mutant tau were destained with 30% methanol for 4 h. Upon reduction (10 mM DTT) and alkylation (65 mM 2-chloroacetamide) of cysteines, proteins were digested overnight with 500 ng of sequencing-grade modified trypsin (Promega) at 37°C. Peptides were extracted by incubating the gel with 150 μl of 50% acetonitrile/0.1% trifluoroacetic acid (TFA) for 30 min at room temperature. A second extraction with 150 μl of 100% acetonitrile/0.1% TFA was also performed. Both extracts were combined and dried in a Vacufuge (Eppendorf).

Mass spectrometry. Resulting peptides were dissolved in 9 μl of 0.1% formic acid/2% acetonitrile solution (to achieve ~500 ng peptide/μl), and 2 μl of the peptide solution was resolved on a nano-capillary reverse-phase column (2 μm, 50 cm; Acclaim PepMap C18, Thermo Fisher Scientific) using a 0.1% formic acid/2% acetonitrile (Buffer A) and 0.1% formic acid/95% acetonitrile (Buffer B) gradient at 300 nl/min over a period of 90 min (2–25% buffer B in 45 min, 25–40% in 5 min, and 40–90% in 5 min followed by holding at 90% buffer B for 5 min and re-equilibration with Buffer A for 30 min). Eluent was directly introduced into the Orbitrap Fusion Tribrid Mass Spectrometer (Thermo Fisher Scientific) using an EasySpray source. MS1 scans were acquired at 120K resolution (automatic gain control (AGC) target = 1×10^6; maximum injection time (IT) = 50 ms). Data-dependent collision-induced dissociation tandem mass spectrometry (MS/MS) spectra were acquired using top speed method (3 s) following each MS1 scan (normalized collision energy (NCE), ~32%; AGC target = 1×10^5; maximum IT, 45 ms).

Database search. Proteins were identified by searching the data against the mouse protein database (17,417 entries; reviewed and downloaded on May 6, 2020) using Proteome Discoverer (version 2.4; Thermo Fisher Scientific). Search parameters included MS1 mass tolerance of 10 ppm and fragment tolerance of 0.1 Da; two missed cleavages were allowed; carbamidimethylation of cysteine was considered as a fixed modification. Oxidation of methionine; deamidation of aspergine and glutamine, diglycine remnant, or acetylation on lysine; phosphorylation on serine, threonine, and tyrosine were considered as potential modifications. Fixed peptide-spectrum match validator of the Proteome Discoverer was used to retain only higher-quality PSMs (ΔC, $n \geq 0.05$). All PSMs corresponding to the modified peptides were verified manually. The abundance of post-translational modifications was normalized to the abundance in nontransgenic mice and analyzed using Student's *t* test.

Experimental design and statistical analyses

For mouse genetic crosses, a two-tailed power analysis using Cohen's Power Table ($\alpha = 0.05$) revealed that a sample size of $n = 4$ would allow us to detect a densitometry difference by Western blot between groups 80% of the time. To sufficiently power experiments to detect sex-dependent effects, a sample size of $n = 3$–7 male and female mice (total, 6–14 mice) was used per group for survival analyses. After evaluating that no significant sex differences existed in tau pathology, a sample size of two to four male and female mice (total, four to eight) per group was used for protein analyses. All Western blot, immunofluorescence, and qPCR analyses were repeated in triplicate, and statistical analyses used means from the three replicates. The accepted level of significance for all analyses was $p \leq 0.05$. All analyses comparing two groups were analyzed using Student's *t* test, and comparisons among three or more groups were completed by one-way ANOVA and the Tukey's *post hoc* test for normal distributions and the Kruskal–Wallis test for non-normal distributions. Data are expressed as the mean ± SEM with individual data points overlaid. *p*-Values for overall ANOVAs are displayed in analyses that did not show any significant differences, and individual *post hoc* comparison *p*-values are displayed for significant ($p < 0.05$) comparisons. Correlation between age and tau levels and UBQLN2 deposition in tau transgenic mice was completed using linear regression analysis. For survival analysis, a Kaplan–Meier plot is shown, and data were analyzed using the Mantel–Cox test. Data were analyzed in StatView (SAS Institute), GraphPad Prism 7, or R.

Results

Among brain-expressed ubiquilins, UBQLN2 markedly decreases tau levels in cell-based assays

UBQLN2 has been linked directly and indirectly to various neurodegenerative diseases, whereas weaker evidence implicates the other brain-expressed ubiquilins, UBQLN1 and UBQLN4 (Smemo et al., 2006; Deng et al., 2011). To determine whether UBQLNs redundantly regulate the disease protein tau, we overexpressed or knocked down UBQLN1, 2, or 4 in HEK293 cells while coexpressing wild-type 0N4R tau. Total tau levels were significantly decreased by UBQLN2 expression ($p < 0.006$; Fig. 1*A*); conversely, tau levels were increased by UBQLN2 knockdown ($p = 0.003$; Fig. 1*B*). In contrast, UBQLN1 overexpression did not decrease tau levels as robustly as UBQLN2, and UBQLN1 knockdown had no effect on tau levels (Fig. 1*A*,*B*). Immunoprecipitation of FLAG-tagged UBQLN2 captured tau from transgenic mice overexpressing tau and UBQLN2, supporting a physical interaction between tau and UBQLN2 (Fig. 1*C*). To exclude the possibility that interactions between different UBQLNs or compensation for the loss of a single UBQLN might influence results, we determined that knocking down UBQLN1 or UBQLN2 did not reciprocally alter levels of the other UBQLN (Fig. 1*D*,*E*). In contrast to UBQLN2, UBQLN4 (Fig. 1*F*) did not alter total tau levels when overexpressed or knocked down, measured by Western blot (UBQLN4 overexpression or knockdown, $p = 0.61$ and $p = 0.09$, respectively). To

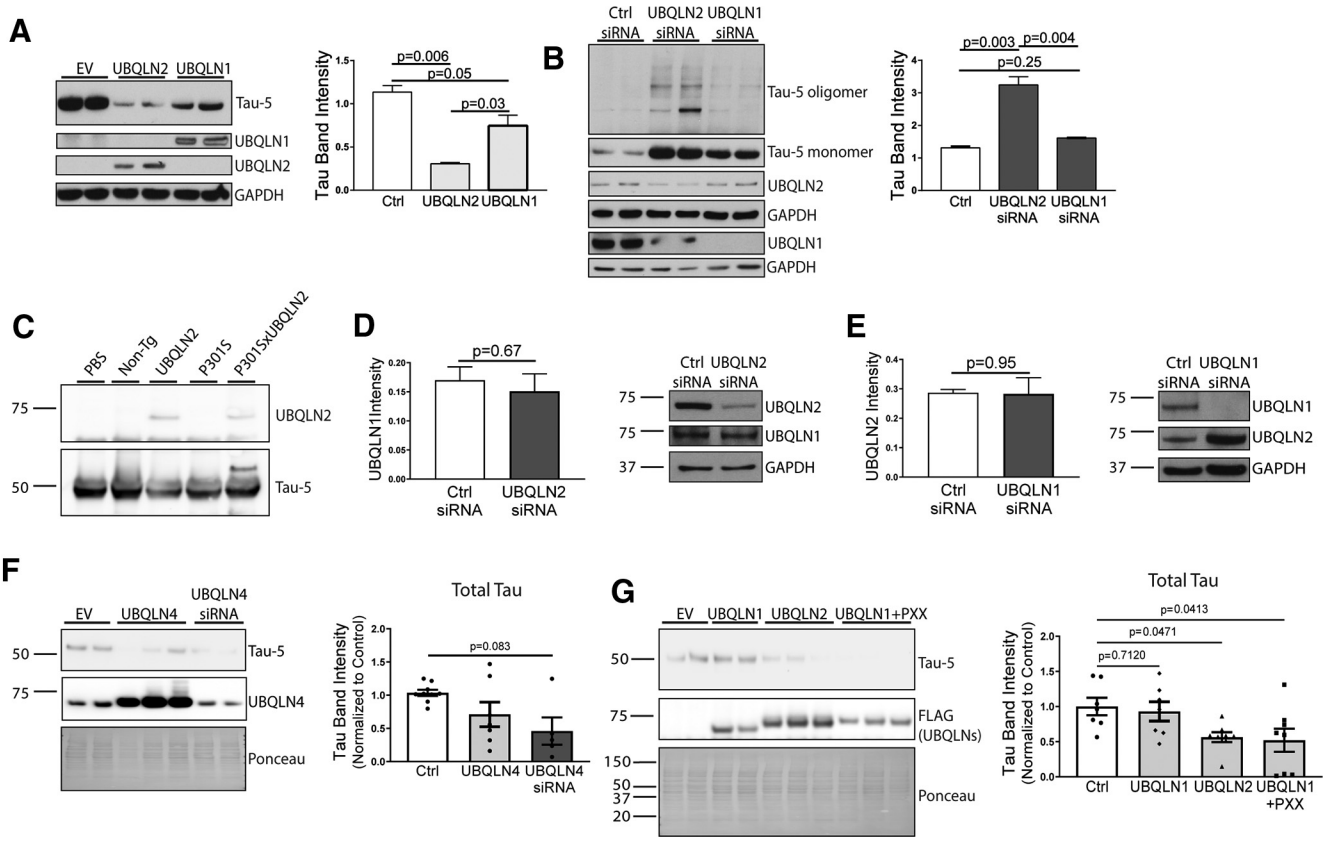

Figure 1. Among UBQLNs, UBQLN2 preferentially lowers wild-type tau levels in HEK293 cells. ***A***, Overexpressed UBQLN2 decreases total tau levels significantly more than does overexpressed UBQLN1 ($n \geq 7$). ***B***, UBQLN2 siRNA knockdown increases total tau levels, whereas UBQLN1 siRNA knockdown has no effect on tau levels. ***C***, Tau is pulled down with FLAG-tagged UBQLN2 when immunoprecipitated from transgenic mice overexpressing both proteins ($n = 2$). ***D***, ***E***, Knockdown of UBQLN2 or UBQLN1 does not alter levels of the reciprocal nontargeted UBQLN ($n = 6$). ***F***, Total tau levels are not significantly altered by coexpression or knockdown of UBQLN4 ($n \geq 5$). ***G***, Inserting the UBQLN2-PXX domain into UBQLN1 leads to decreased tau levels ($n \geq 7$).

assess why UBQLN2 selectively handles tau, we inserted the proline-rich (PXX) domain, which is unique to UBQLN2, into UBQLN1. Inserting the PXX domain into UBQLN1 led to a marked decrease in tau levels that was not seen with wild-type UBQLN1 ($p = 0.0413$; Fig. 1*G*).

To investigate UBQLN effects on tau levels and cellular localization, we measured tau by immunofluorescence in HEK293 cells expressing tau together with expression or knockdown of UBQLN1 or UBQLN2. The fraction of tau-positive cells was significantly decreased by UBQLN2 expression ($p = 0.006$) and increased by UBQLN2 knockdown ($p = 0.0004$; Fig. 2*A*,*C*). In contrast, modulating UBQLN1 levels did not significantly change the number of tau-positive cells (UBQLN1 overexpressed, $p = 0.34$; UBQLN1 knocked down, $p = 0.25$; Fig. 2*B*,*D*). To control for potential differences in transfection efficiency between UBQLN1 and UBQLN2, we compared the ratio of tau-positive cells to UBQLN1-positive or UBQLN2-positive cells. Tau-positive cells were significantly decreased when expressed as a ratio to UBQLN2-positive cells compared with UBQLN1-positive cells ($p = 0.02$; Fig. 2*E*). To establish that these differences reflect changes in the handling of tau protein rather than tau expression at the RNA level, we verified that tau transcript levels were unchanged by UBQLN2 expression ($p = 0.54$; Fig. 2*F*).

Tau-expressing transgenic mice display an age-dependent increase in insoluble UBQLN2

Our cell culture results imply that UBQLN2, but not other UBQLNs, regulates tau protein levels. To further determine the physiological relevance of UBQLN2 to tau homeostasis, we extended our analysis to tau transgenic mouse models. The intrinsic property of UBQLN2 to aggregate (Hjerpe et al., 2016; Sharkey et al., 2018; Gerson et al., 2021), combined with our results showing that UBQLN2 knockdown increased levels of wild-type tau, suggested that UBQLN2 aggregation might promote tau pathology. We also sought to determine whether tau pathology, in turn, could contribute to a cellular environment that enhances the tendency of UBQLN2 to aggregate and hence become dysfunctional. To investigate this possibility, we assessed UBQLN2 levels from brain homogenates of a widely used tau transgenic mouse model that expresses wild-type Htau isoforms (Andorfer et al., 2003). High-molecular weight (HMW) UBQLN2, presumably reflecting aggregated UBQLN2, increased in aged Htau mice, paralleling both an increase in tau pathology and signs of neurodegeneration (Fig. 3*A*). Non-Tg littermates and transgenic mice overexpressing FTD mutant tau (P301S; Yoshiyama et al., 2007) were also collected and similarly analyzed. While an increase in HMW UBQLN2 was exclusive to Htau transgenic mice, soluble monomeric UBQLN2 levels increased as a function of both age and P301S tau genotype (Fig. 3*B*). By contrast, UBQLN1 and UBQLN4 levels were unchanged. To determine whether tau pathology is associated with the accumulation of UBQLN2, we assessed endogenous UBQLN2 immunofluorescence in P301S and nontransgenic mice in various brain regions (Fig. 3*C*). P301S mice displayed heterogeneity in UBQLN2 staining consistent with the accumulation of insoluble UBQLN2 in a subset of cells, although overall UBQLN2 fluorescence intensity was unchanged by tau genotype.

To determine whether UBQLN2 levels were also altered in human tauopathy cases, we assessed UBQLN2 in soluble and

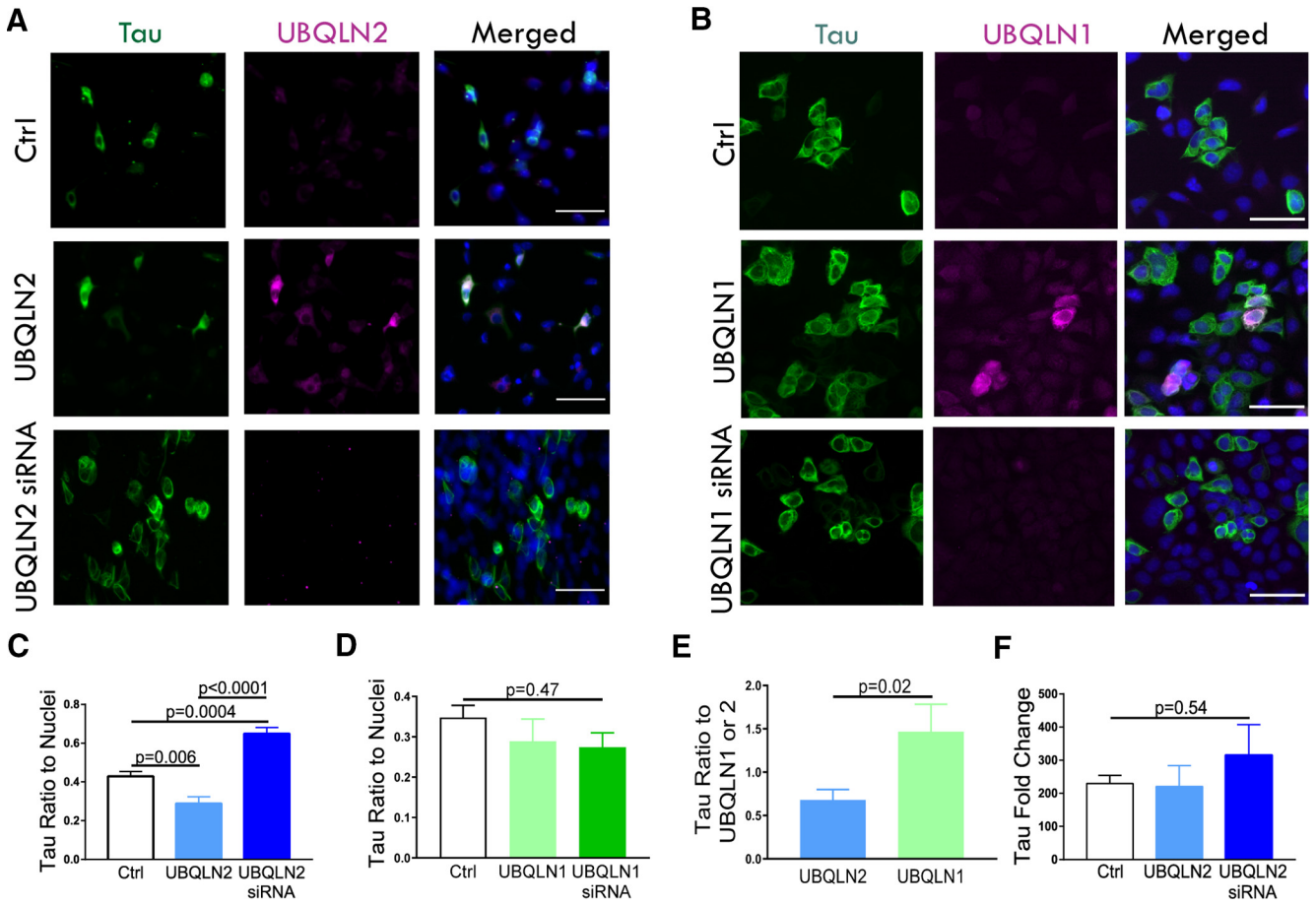

Figure 2. Immunofluorescence shows that UBQLN2 preferentially decreases wild-type tau protein. ***A***, ***C***, Tau-positive cells are significantly decreased by UBQLN2 coexpression and increased by UBQLN2 knockdown ($n = 10$ fields of view from three coverslips, 150–200 cells/group). ***B***, ***D***, In contrast, UBQLN1 expression does not change tau levels ($n = 10$ fields of view from three coverslips, 150–200 cells/group). ***E***, There are significantly more tau-positive cells expressed as a ratio to UBQLN1-positive cells than to UBQLN2-positive cells. ***F***, Tau transcript levels are not significantly changed by UBQLN2 expression or knockdown, assessed by qRT-PCR ($n = 10$). Scale bar, 100 μm.

insoluble brain homogenates of frontal cortex from nondemented (control) and cases of PSP, an established human tauopathy. PSP brain extracts exhibited increased levels of HMW UBQLN2 compared with control brains (Fig. 3*D*). Compared with female PSP samples, male PSP samples showed a trend toward increased insoluble UBQLN2, suggesting a potential sex difference in UBQLN2 expression in disease that warrants further investigation. Our results imply that while UBQLN2 overexpression may directly reduce tau levels in cells, the observed increase in potentially nonfunctional HMW and insoluble UBQLN2 in disease states could render the cellular pool of UBQLN2 less capable of regulating tau because of the propensity of UBQLN2 to aggregate.

Altering UBQLN2 levels in a tauopathy mouse model modulates tau phosphorylation status

To test the extent of tau regulation by UBQLN2 *in vivo,* we crossed mouse lines with varying UBQLN2 levels to the P301S tauopathy mouse model. UBQLN2-Hi Tg or UBQLN2 KO mice were crossed with P301S tau mice (Fig. 4*A*), then total tau levels were assessed in 9-month-old whole-brain homogenates. While total tau levels were not significantly changed by UBQLN2 overexpression or knockout (Fig. 4*B*,*C*), a slower migrating form of tau [denoted with an asterisk (*)] consistent with AT8 hyperphosphorylated tau appeared in P301S mice overexpressing UBQLN2 (Fig. 4*B*). Conversely, in P301S mice lacking UBQLN2, total tau immunofluorescence trended downward in the hippocampus and prefrontal cortex (PFC), the two main brain regions associated with a high degree of tau pathology (Fig. 4*D*,*E*). Similarly, we find that UBQLN2 expression did not affect total levels or the turnover of wild-type tau in primary rat cortical neurons (Fig. 4*F*,*G*).

Contrary to our HEK cell-based results (Figs. 1, 2), the above results suggest UBQLN2 *in vivo* may actually promote an increase in post-translationally modified tau. Using antibodies specific for human tau and phosphorylated tau, we confirmed that UBQLN2 overexpression increases levels of phosphorylated tau species that migrate more slowly in SDS-PAGE with increased phosphorylation at several sites, as well as HMW/oligomeric species (Fig. 5*A*). Soluble and insoluble pS202/Thr205 and pThr231, as well as soluble pS396 tau monomer, are all significantly increased in P301SxUBQLN2-Hi mice (Fig. 5*B*,*C*). Total levels of tau phosphorylated at S262 and S356 are also increased when UBQLN2 is overexpressed (data not shown). Conversely, P301S mice lacking UBQLN2 showed significantly decreased levels of soluble pS202 tau oligomer and 37 kDa tau fragment, as well as a trend toward decreased pThr231 tau monomer (Fig. 5*B*).

To directly evaluate changes to tau phosphorylation, we immunoprecipitated tau from 9-month-old Non-Tg, P301S, and P301SxUBQLN2-Hi mice (Extended Data Fig. 5-1) and analyzed

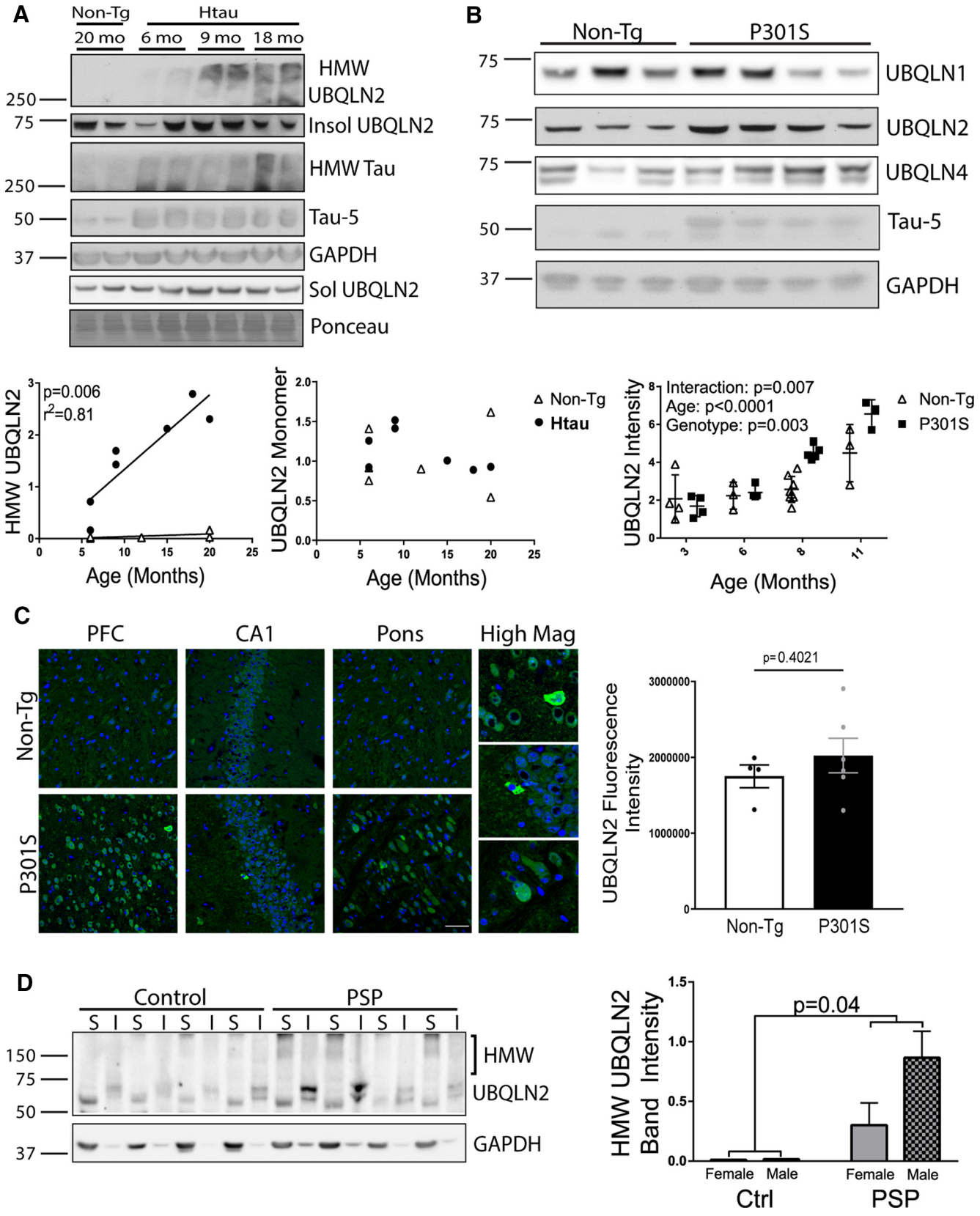

Figure 3. Linked dysregulation of tau and UBQLN2 in tauopathy animal models and human disease tissue. ***A***, Levels of HMW UBQLN2 increase over time in human wild-type tau-expressing (Htau) mice, and correlate with age-related increases in tau pathology ($n = 3$/age group), while UBQLN2 monomer does not significantly differ between groups. ***B***, Western blot analysis of brain lysates from 8-month-old mice shows an increase of soluble UBQLN2 in P301S tau transgenic mice. With age, soluble UBQLN2 levels increase in both Non-Tg and P301S tau mice ($n = 5$/age group). ***C***, Endogenous UBQLN2 immunofluorescence (green) in PFC, hippocampal CA1 region, and pons of 9-month-old Non-Tg and P301S mice. Higher-magnification images reveal heterogeneous, increased UBQLN2 labeling in a subset of neurons in P301S mice. Overall UBQLN2 fluorescence intensity, however, does not differ significantly between P301S and Non-Tg mice, shown here for PFC ($n \geq 3$/group). ***D***, Fractionation of mid-frontal gyrus lysate into PBS-soluble (S) and Sarkosyl soluble (I) fractions reveals elevated insoluble HMW UBQLN2 in PSP brain

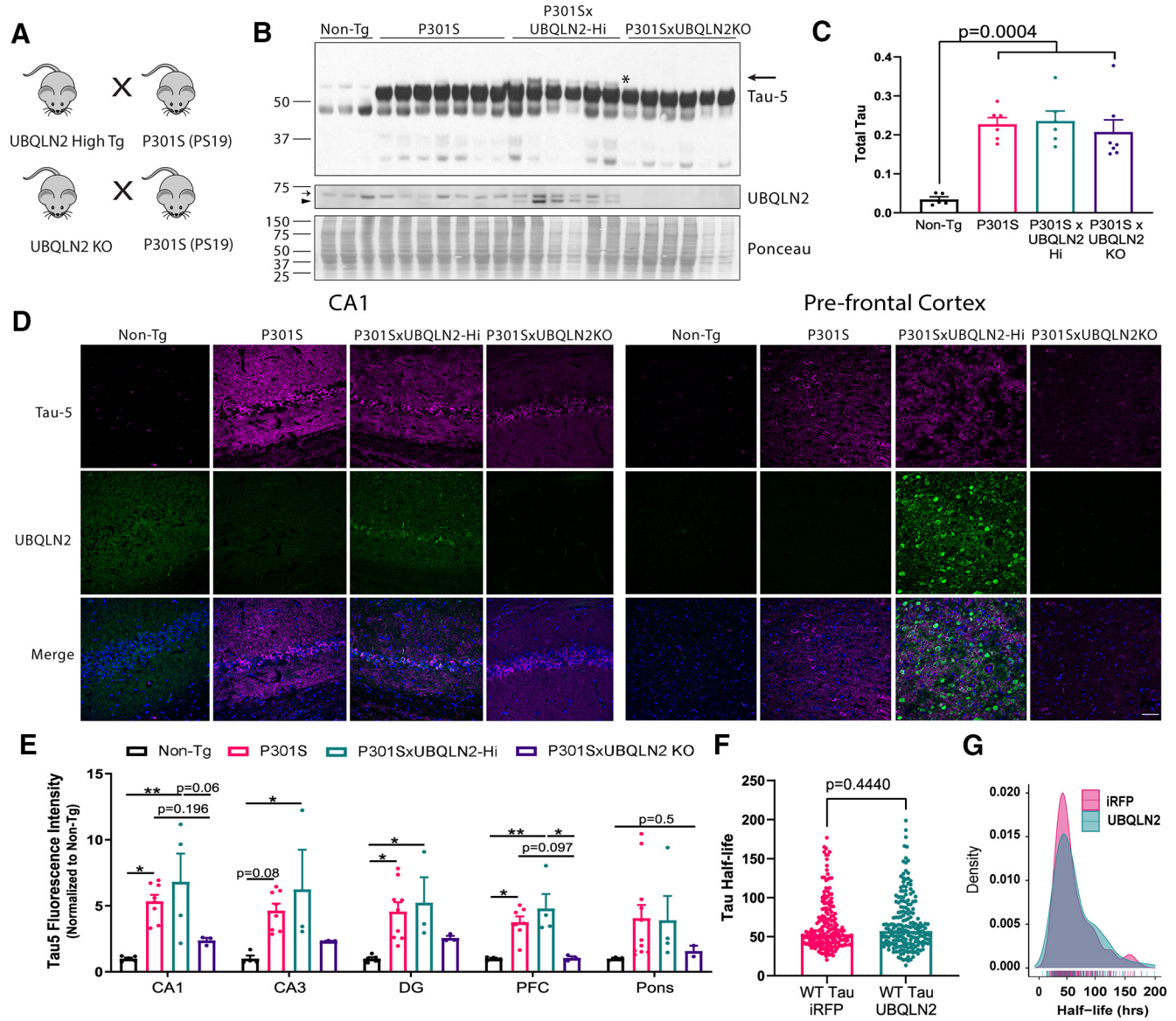

Figure 4. UBQLN2 increases slow-migrating tau species consistent with tau phosphorylation, while knocking out UBQLN2 lowers tau in the frontal cortex. ***A***, Breeding strategy to produce P301S mice expressing mutant tau alone and with UBQLN2 overexpressed or knocked out. ***B***, Whole-brain RIPA lysates from 9-month-old Non-Tg, P301S, P301SxUBQLN2-Hi transgenic, and P301SxUBQLN2 KO mice probed with the pan-tau antibody Tau-5 reveal a more slowly migrating tau species present only when UBQLN2 is overexpressed (labeled with an asterisk and arrow). Western blot was also probed with UBQLN2 antibody (arrow labels endogenous murine UBQLN2; arrowhead labels transgenic human UBQLN2) and Ponceau S stain for total protein. ***C***, Total Tau-5 levels normalized to Ponceau S are similarly increased in P301S mice regardless of UBQLN2 expression ($n \geq 5$/group). ***D***, Total tau (Tau-5, magenta) and UBQLN2 (green) immunofluorescence in the hippocampal CA1 region and PFC of 9-month-old Non-Tg, P301S, P301SxUBQLN2-Hi, and P301SxUBQLN2 KO mice. ***E***, Quantification of total tau immunofluorescence in the CA1, CA3, and dentate gyrus (DG) of the hippocampus and the PFC reveals similar elevated tau in P301S and P301SxUBQLN2-Hi mice, whereas P301SxUBQLN2 KO mice show a decrease in total tau that approaches levels in Non-Tg mice ($n \geq 3$/group; Extended Data Table 4-1, statistical details). Immunofluorescent images for CA3, DG, and pons are in Extended Data Figure 4-1. Scale bar, 50 μm. ***F***, Optical pulse labeling in primary rat neurons reveals no change in the half-life of tau-Dendra2 on transfection with UBQLN2 versus control (iRFP). ***G***, Density plot of tau-Dendra2 half-life measurements from individual neurons transfected with control ($n = 202$) or UBQLN2 ($n = 211$). Values were pooled from eight wells per condition, from each of two biological replicates. Representative images are shown in Extended Data Figure 4-2.

it by MS/MS. We identified multiple tau residues with increased phosphorylation in P301SxUBQLN2-Hi mice (Fig. 5*D*). Confocal immunofluorescence imaging for pS202/Thr305 tau revealed increased phosphorylated tau pathology in the hippocampus, PFC, and pons of 9-month-old P301SxUBQLN2-Hi mice compared with P301S mice (Fig. 6*A–C*, Extended Data Fig. 6-1). This increased phosphorylated tau appeared as early as 6 months, whereas the decrease in phosphorylated tau conferred by UBQLN2 KO appeared by 9 months of age (Extended Data Fig. 6-2).

Intriguingly, the increase in phosphorylated tau associated with UBQLN2 expression in P301SxUBQLN2-Hi mice was observed primarily in neurons residing next to neurons harboring high levels of UBQLN2 (Fig. 6*D*). UBQLN2 and phosphorylated tau only rarely colocalized in the same neuron regardless of brain region, including hippocampus (Fig. 6*D–F*), PFC, and pons (Extended Data Fig. 6-1).

←

compared with age-matched control brain (control, $n = 4$; PSP, $n = 12$). ***E***, Coimmunofluorescence for tau NFTs and UBQLN2 shows UBQLN2 accumulation in PSP brain that is distinct from NFTs (mid-frontal gyrus). Scale bar, 50 μm.

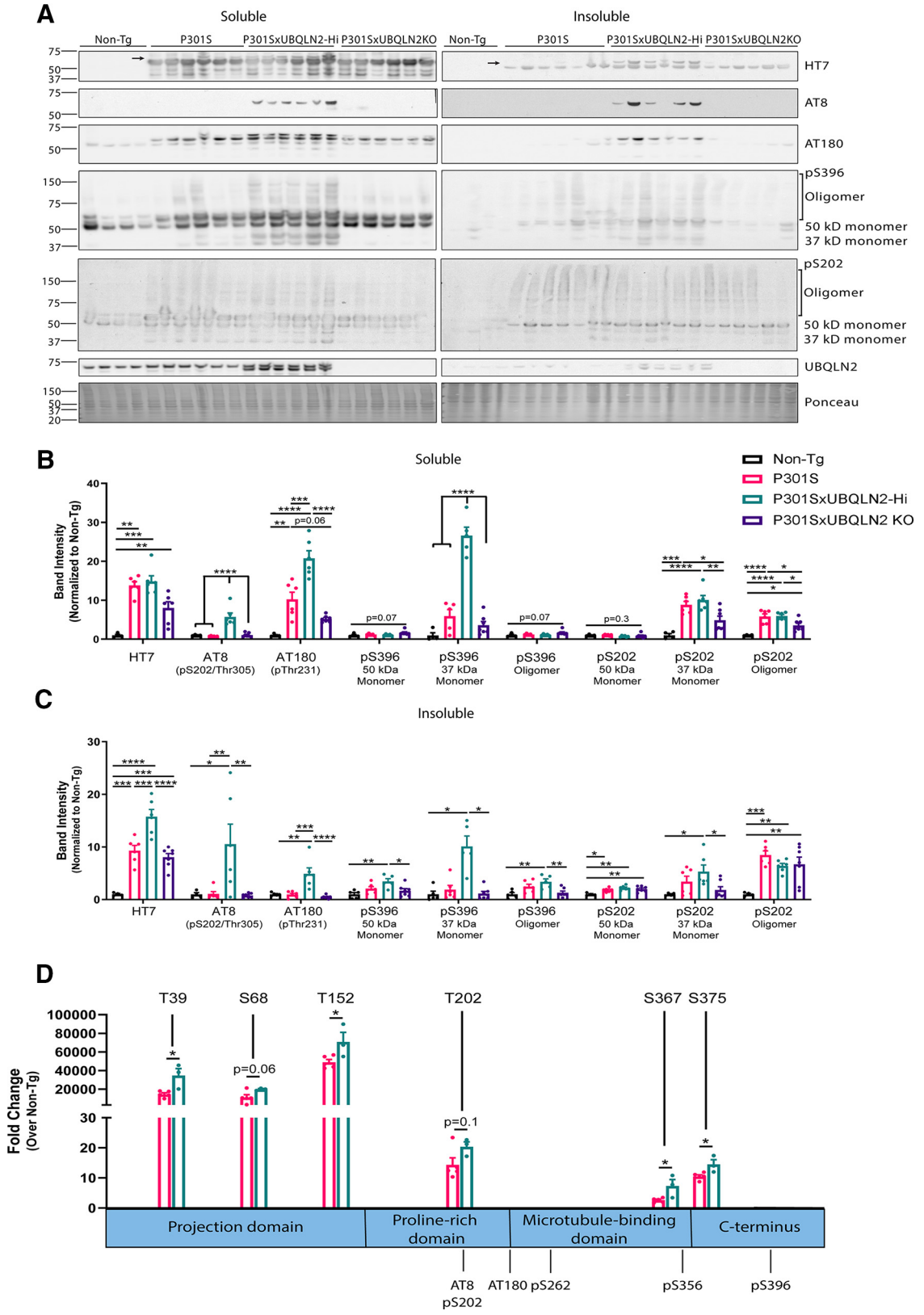

Figure 5. UBQLN2 expression markedly increases phosphorylated tau in P301S tau mice. ***A***, Representative Western blot of soluble (PBS-soluble) and insoluble (Sarkosyl-soluble) fractions of whole-brain lysates from 9-month-old mice of the indicated genotypes, probed with various antibodies, as follows: human tau antibody HT7, the phosphorylated tau epitope-specific antibodies AT8 (pS202, Thr205), AT180 (Thr231), pS396, and pS202, as well as UBQLN2 antibody and Ponceau stain. With HT7 antibody, the arrow labels the higher-molecular weight tau species present when UBQLN2 is overexpressed. ***B***, ***C***, Levels of soluble (***B***) and insoluble (***C***) tau (normalized to Ponceau) reveal a significant increase in phosphorylated tau species at multiple phosphorylation sites when UBQLN2 is overexpressed and a significant decrease when UBQLN2 is knocked out ($n = 4$–7/group; Extended Data Table 5-2, statistical details). ***D***, Fold change over Non-Tg of tau phosphorylation, identified by mass spectroscopy aligned with locations of phospho-epitope-specific tau antibodies. UBQLN2 overexpression increases phosphorylation at all identified sites ($n = 3$–5). Immunoprecipitation data are included in Extended Data Figure 5-1, and statistical details in Extended Data Table 5-1.

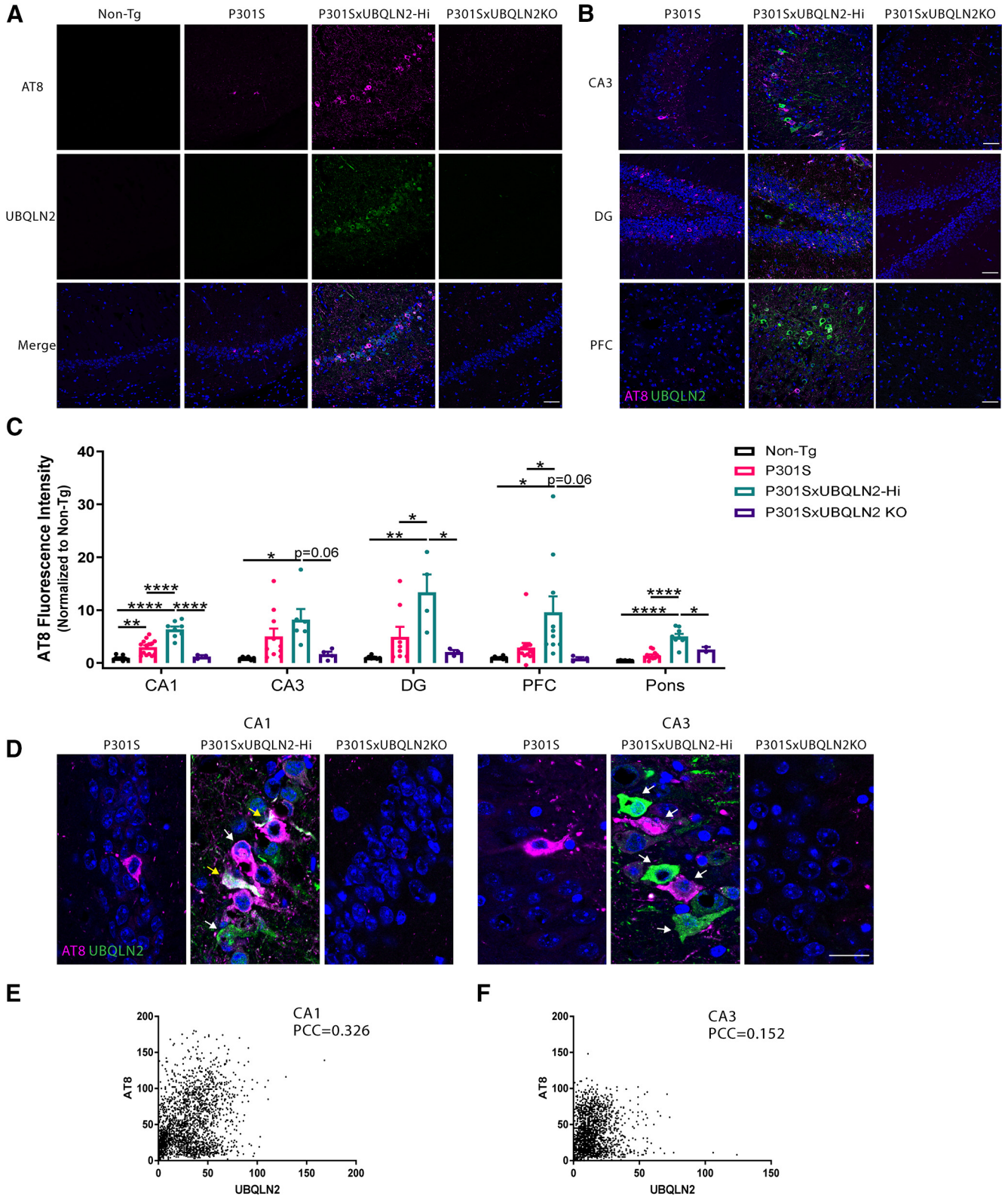

Figure 6. UBQLN2 expression often correlates with increased phosphorylated tau in neighboring cells. ***A***, ***B***, Phosphorylated tau (pS202, pThr205) and UBQLN2 immunofluorescence of the hippocampal CA1 region (***A***) and the CA3, DG, and PFC of 9-month-old Non-Tg, P301S, P301SxUBQLN2-Hi, and P301SxUBQLN2 KO mice (***B***). Scale bar, 50 μm. ***C***, Corrected total AT8 fluorescence intensity in the indicated brain regions is elevated in mice overexpressing UBQLN2, whereas phosphorylated tau levels in P301SxUBQLN2 KO mice do not differ from Non-Tg mice ($n = 3$–12/group; Extended Data Table 6-1, statistical details). ***D***, Magnified images from CA1 and CA3 regions in P301S, P301SxUBQLN2-Hi, and P301SxUBQLN2 KO mice labeled with AT8 (magenta) and UBQLN2 (green). In P301SxUBQLN2 images, yellow arrows highlight coincident staining for AT8 and UBQLN2, whereas white arrows indicate cells labeled with only UBQLN2 or AT8. Scale bar, 25 μm. UBQLN2 and AT8 fluorescence colocalized only ~10.6% of the time in the CA1, PFC, and pons, and only ~2.2% of the time in the CA3. ***E***, ***F***, Scatter plots of UBQLN2-positive versus AT8-positive pixels in CA1 and CA3 regions of P301SxUBQLN2-Hi mice. Complete CA3, PFC, DG, and pons images are in Extended Data Figure 6-1. Increased phosphorylated tau levels driven by UBQLN2 overexpression can be detected starting at 6 months of age (Extended Data Fig. 6-2, 3–6 months of data).

UBQLN2 aggregation is not required for UBQLN2-mediated increase in tau phosphorylation

To rule out the possibility that the observed tau changes in UBQLN2-Hi mice are simply a by-product of increased aggregation of overexpressed UBQLN2, we conducted additional genetic crosses with a transgenic mouse line expressing much less UBQLN2 (UBQLN2-Low). In UBQLN2-Low mice, UBQLN2 remains soluble and diffusely distributed (Sharkey et al., 2020). Again, both soluble and insoluble phosphorylated tau (pS202/Thr205 and pThr231 tau) were significantly increased in P301SxUBQLN2-low mice compared with P301S mice (Fig. 7*A*,*B*). Likewise, increases in phosphorylated tau assessed by immunofluorescence were detected in the hippocampus and PFC (Fig. 7*C*,*D*) in a similar, albeit less robust, pattern as in P301SxUBQLN2-Hi. These results suggest that the action of UBQLN2 on tau is both dose dependent and not contingent on UBQLN2 aggregation.

Expanding on our earlier results showing that tau pathology is associated with increased high-molecular weight and insoluble UBQLN2, we evaluated whether UBQLN2 puncta formation in neurons is promoted by P301S tau expression in UBQLN2-high mice. Quantification of the number of puncta per cell across the frontal cortex, CA1, CA3, DG, and pons revealed no change in UBQLN2 puncta formation in UBQLN2-Hi mice, with or without pathologic tau overexpression (Fig. 7*E*).

UBQLN2 differentially handles distinct forms of tau

To determine whether UBQLN2 overexpression alters levels of wild-type endogenous tau *in vivo*, we analyzed levels of endogenous murine tau in PBS-soluble and PBS-insoluble fractions of brain lysates from Non-Tg and UBQLN2-Hi mice. Insoluble tau was significantly decreased in UBQLN2-Hi mice ($p = 0.05$), whereas soluble tau was not altered ($p = 0.5$; Fig. 8*A*). These results suggest UBQLN2 action reduces the accumulation of insoluble wild-type tau without broadly reducing total soluble and presumably natively folded endogenous tau.

To gauge the effect of UBQLN2 on tau aggregation intermediates that may promote tau toxicity, we used the conformational antibody Alz50 to measure soluble, misfolded tau species by dot blot in nondenatured brain homogenate. UBQLN2 expression caused a downward trend in levels of endogenous murine misfolded tau protein, whereas P301S mice crossed to both UBQLN2-Low and UBQLN2-Hi mice had increased levels of misfolded P301S mutant human tau, trending above levels seen with P301S tau expression alone (Fig. 8*B*).

Based on our results in mouse brain suggesting differential regulation of wild-type and mutant tau by UBQLN2, we sought to determine whether UBQLN2 differentially regulates wild-type and P301S mutant tau in HEK cells. Similar to wild-type 0N4R tau, wild-type 2N4R tau was significantly increased when UBQLN2 was knocked down, while UBQLN2 had no effect on levels of P301S 2N4R tau (Fig. 8*C*), providing further evidence supporting a divergent role of UBQLN2 in regulating different forms of tau.

UBQLN2 overexpression exacerbates tau toxicity

The robust effect of UBQLN2 on tau pathology in P301S mice prompted us to determine whether tau-mediated toxicity exacerbated by UBQLN2 manifested as a change in survival. Indeed, both P301SxUBQLN2-Low and P301SxUBQLN2-Hi mice were significantly less likely to survive to 9 months compared with all other groups (Fig. 9*A*). Furthermore, by 9 months a subset of P301SxUBQLN2-Low and P301SxUBQLN2-Hi mice acquired premature hindlimb paralysis that did not occur in P301S mice (Fig. 9*B*). This reduced survival was not preceded by behavioral and motor changes at 6 months of age, assessed by Open Field and Novel Object Recognition tests (data not shown); based on the survival data, we surmise that 6 months may be too early to detect differences. To confirm that changes in phosphorylated tau (Figs. 5, 6) resulted in an accumulation of neurofibrillary tangles (NFTs), we used Thioflavin-S staining to measure the NFT burden in the prefrontal cortex. As anticipated, UBQLN2 overexpression in the P301S model (P301SxUBQLN2-Hi) was associated with markedly increased Thioflavin-S-positive NFTs (Fig. 9*C*). To probe whether NFTs occur primarily in cells lacking UBQLN2, we colabeled P301SxUBQLN2 brains with anti-UBQLN2 and Thioflavin S. Consistent with our results for phosphorylated tau, we found that NFTs in the hippocampus and frontal cortex also occur in cells lacking UBQLN2 accumulation (Fig. 9*D*).

UBQLN2 and tau pathology are associated with changes to proteostasis proteins

To test whether disrupting the balance of UBQLN2 broadly dysregulates proteostasis pathways, we measured levels of various PQC pathway markers in 9-month-old Non-Tg, P301S, P301SxUBQLN2-Hi, and P301SxUBQLN2-KO mice in whole-brain lysate (Fig. 10*A*,*B*). Given that wild-type, but not mutant, tau is a substrate for CMA and given the known role of macroautophagy in reducing tau aggregates, we probed for changes to CMA and macroautophagy by measuring levels of LAMP2A, LC3A, and p62. LAMP2A levels were increased and LC3A levels were significantly reduced when UBQLN2 was either overexpressed or knocked out, suggesting that disrupting the balance of UBQLN2 dysregulates autophagy pathways. Both tau and UBQLN2 aggregates have been shown to colocalize with p62 (Kuusisto et al., 2002; Sharkey et al., 2020), which may facilitate targeting them for degradation, but neither mutant tau nor UBQLN2 expression changed total p62 levels. Based on previous data showing that p62 puncta formation is increased in UBQLN2 mice in the absence of changes to overall p62 levels (Sharkey et al., 2020) or other autophagy proteins, we measured p62 (Fig. 10*D*,*E*, Extended Data Fig. 10-1) and LAMP2A (Fig. 10*G*,*H*, Extended Data Fig. 10-1) puncta. P301SxUBQLN2-Hi mice have increased p62 and LAMP2A puncta formation, suggesting that UBQLN2 disrupts the facilitation of p62-mediated clearance and may mediate CMA activity. P301SxUBQLN2 KO mice also display elevated levels of p62 puncta. These results suggest that p62 puncta do not solely reflect accumulation in UBQLN2 aggregates but represent an overall imbalance in autophagy and ubiquitin-dependent protein clearance.

UBQLN2 is known to shuttle ubiquitinated proteins to the proteasome and interact with molecular chaperones that may assist tau clearance by CMA (Hjerpe et al., 2016; Zhang et al., 2021). Accordingly, we measured levels of ubiquitin, the molecular chaperones Hsp70 and Hsp90B, and the cochaperone FKBP5 involved in regulating tau. Ubiquitin levels were significantly increased in P301SxUBQLN2-Hi mice over all other groups, further supporting the idea that an imbalance in UBQLN2 disrupts ubiquitin-dependent protein regulatory pathways. To test whether tau ubiquitination is increased by UBQLN2 overexpression, we measured levels of ubiquitin associated with tau immunoprecipitated from 9-month-old Non-Tg, P301S, and P301SxUBQLN2-Hi transgenic mouse brain, and

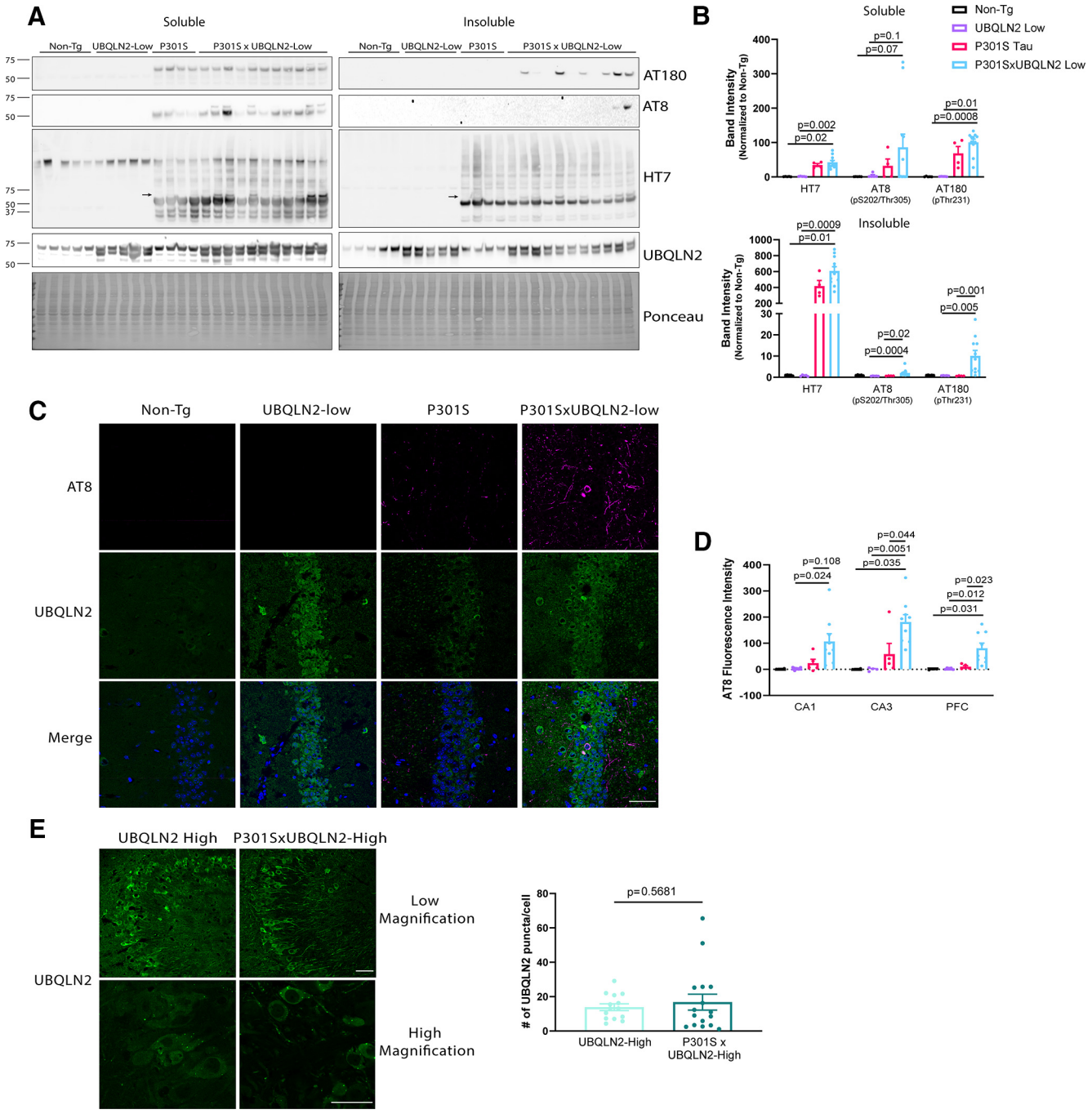

Figure 7. UBQLN2 aggregation is not the basis for the UBQLN2-mediated increase in tau phosphorylation. ***A***, Representative Western blot of soluble (PBS-soluble) and insoluble (Sarkosyl-soluble) fractions of whole-brain lysates from 9-month-old Non-Tg, UBQLN2 Low, P301S, and P301SxUBQLN2-Low mice probed with human tau antibody (HT7) and phosphorylated tau epitope-specific antibodies, AT8 (pS202, Thr205) and AT180 (Thr231), UBQLN2 antibody, and Ponceau stain. ***B***, Even when UBQLN2 is overexpressed at low levels, insoluble phosphorylated tau is still increased, as measured by AT8 and AT180 antibodies. In contrast, soluble and insoluble human tau and soluble phosphorylated tau do not differ with low UBQLN2 overexpression ($n = 4$–11/group). ***C***, AT8 and UBQLN2 immunofluorescence in the CA1 hippocampus of 9-month-old mice with the indicated genotypes. ***D***, Phosphorylated tau is increased in P301SxUBQLN2-Low mice over P301S mice in hippocampus and frontal cortex ($n = 5$–9). ***E***, UBQLN2 immunofluorescence in CA3 revealed no significant differences in UBQLN2 puncta per cell between UBQLN2-Hi and P301SxUBQLN2-Hi mice. Scale bar, 50 μm.

found no changes to tau ubiquitination (Fig. 10*C*). Assessed by immunofluorescence, the accumulation of poly-ubiquitin does not primarily localize to phosphorylated tau (Fig. 10*F*, Extended Data Fig. 10-1). Thus, this increase in ubiquitin is not simply a by-product of a failure to degrade ubiquitinated tau. No significant differences were seen in total levels of Hsp70 or Hsp90B, but FKBP5 increased when UBQLN2 was both overexpressed and knocked out.

The UBQLN2-dependent increase in hyperphosphorylated tau species led us to test whether UBQLN2 affected levels of total and deactivated tau kinase, GSK3β, and pGSK3β. Levels of GSK3β increased and pGSK3β decreased as a function of increased tau pathology (Fig. 10*A*,*B*), as shown previously (Dumont et al., 2011), but were not altered by UBQLN2 per se. An additional tau kinase, MARK2, was unchanged with UBQLN2 expression or knockout in P301S mice (data not

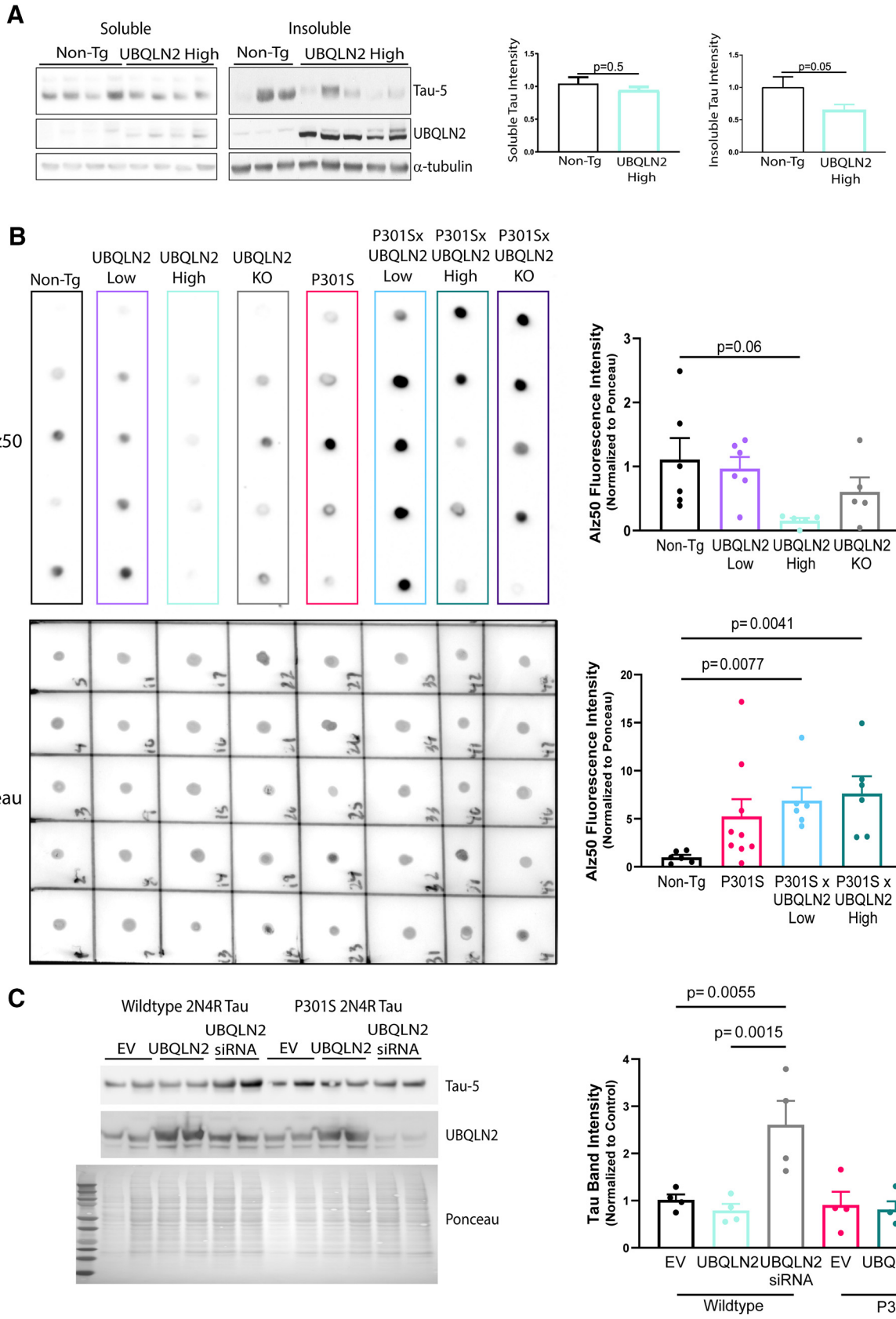

Figure 8. UBQLN2 acts differently on endogenous wild-type tau and overexpressed mutant tau. ***A***, Western blot of soluble (PBS-soluble) and insoluble (Sarkosyl-soluble) fractions of whole-brain lysates from 12-month-old Non-Tg and UBQLN2-high mice probed with the pan-tau antibody Tau-5. Insoluble endogenous tau monomer is significantly decreased in mice overexpressing UBQLN2, whereas soluble tau levels are unchanged ($n = 6$). ***B***, Representative dot blot of soluble, nondenatured whole-brain lysate from mice with the indicated genotypes, probed with the misfolded tau conformational antibody Alz50 and stained with Ponceau. While endogenous murine misfolded tau levels trend lower when UBQLN2 is overexpressed, misfolded mutant human tau levels are increased by UBQLN2 overexpression ($n = 5$–9/group). ***C***, Western blot of total protein cell lysates from HEK cells transfected with full-length wild-type and P301S mutated tau

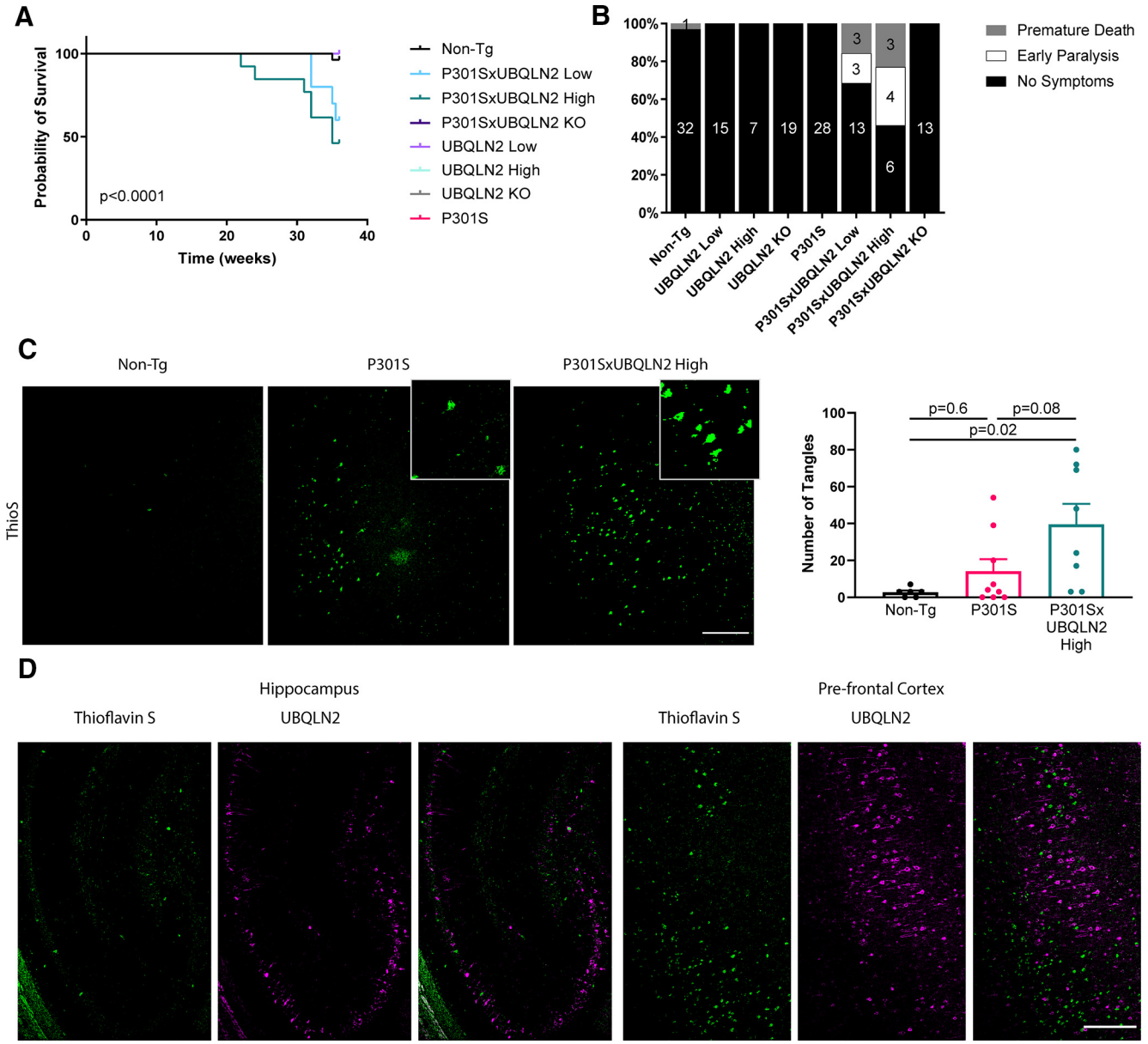

Figure 9. UBQLN2 overexpression exacerbates tau toxicity in P301S mice. ***A***, Kaplan–Meier survival curves demonstrate decreased probability of survival for UBQLN2-Low-expressing and UBQLN2-Hi-expressing mice crossed to P301S mice ($n = 13$–19; Mantel–Cox test, $p < 0.0001$). ***B***, Ratio of mice of indicated genotypes exhibiting early paralysis or premature death (at or before the 9 month collection point). ***C***, Thioflavin S labeling of prefrontal cortex revealed trend toward increased tangle deposition in P301S mice coexpressing UBQLN2 ($n = 3$/group). ***D***, Colabeling of Thioflavin S and UBQLN2 in P301SxUBQLN2 mice. UBQLN2 deposits do not colocalize with NFTs in prefrontal cortex or hippocampus. Scale bar, 200 μM.

shown). These results suggest that UBQLN2-induced changes to phosphorylated tau are not because of an increase in the activity of tau-linked kinases.

Discussion

Accumulation of tau into disease aggregates is associated with several common neurodegenerative disorders, yet how tau is differentially regulated in healthy versus disease states is still poorly understood. UBQLN2 has surfaced as a significant modulator of neurodegenerative disease, but its ability to regulate specific members of a wide range of disease-causing proteins, including tau, remains unknown. Here we used cellular and mouse models as well as human disease tissue to test whether UBQLN2 regulates tau. Our results show that UBQLN2, but not the closely related proteins UBQLN1 or UBQLN4, alters levels of wild-type tau in cellular and mouse models. We further provide evidence that UBQLN2 is dysregulated in tauopathy, based on increased UBQLN2 insolubility in mouse and human disease brains harboring tau pathology. Finally, UBQLN2 overexpression exacerbated P301S mutant tau toxicity in mice, suggesting that UBQLN2 functionally diverges in its ability to regulate wild-type endogenous tau under normal conditions versus mutant or aggregation-prone tau in pathologic conditions.

The association of UBQLN2 with several human neurodegenerative diseases (Deng et al., 2011; Mori et al., 2012) prompted us to test the ability of UBQLN2 to lower levels of tau in

←

protein. UBQLN2 siRNA significantly elevates levels of full-length wild-type tau, while UBQLN2 overexpression and knockdown have no significant effect on levels of full-length P301S tau ($n = 4$).

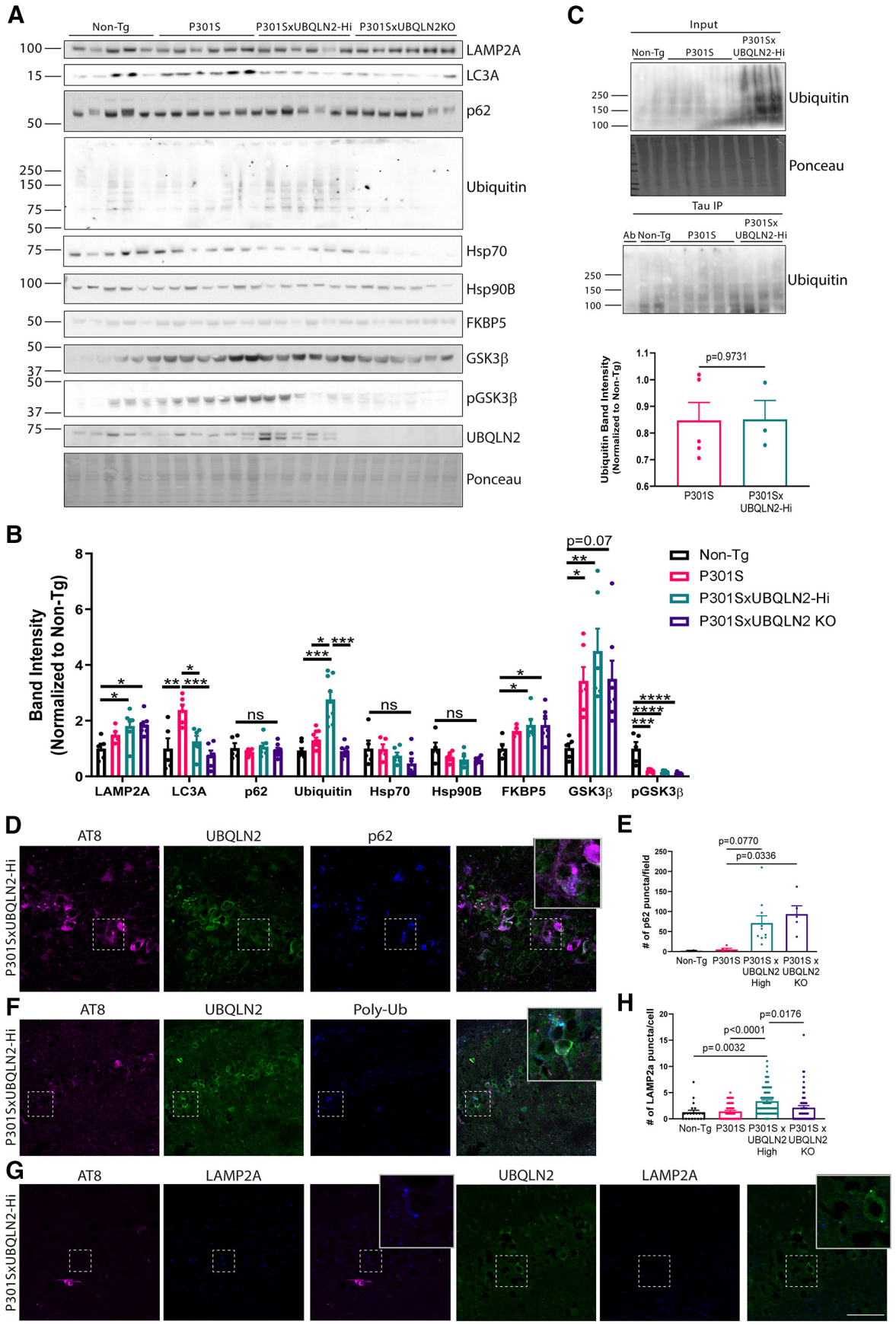

Figure 10. UBQLN2 levels are associated with changes to autophagy protein and poly-ubiquitin levels. ***A***, Whole-brain RIPA lysates from 9-month-old Non-Tg, P301S, P301SxUBQLN2-Hi transgenic, and P301SxUBQLN2 KO mice ($n = 5–7$) were probed with markers for chaperone-mediated autophagy (LAMP2A), macroautophagy (LC3A, p62), ubiquitin, molecular chaperones (Hsp70, Hsp90B, FKBP5), and tau kinases (GSK3β, pGSK3β). ***B***, LC3A levels were significantly lower in both UBQLN2-Hi and UBQLN2 KO crosses to P301S compared with P301S alone, and

HEK293 cells. UBQLN2 expression led to robust decreases in tau whereas knockdown of endogenous UBQLN2 increased tau. This result led us to assess whether this property applies generally to brain-expressed ubiquilins. Whereas UBQLN2 significantly reduced tau levels, UBQLN1 and UBQLN4 did not. This difference suggests that ubiquilins serve distinct functions in the brain and adds to prior work revealing distinct aggregation properties for the three ubiquilins (Gerson et al., 2021). Adding the PXX domain of UBQLN2 to UBQLN1 conferred on UBQLN1 the ability to decrease tau levels, arguing that the proline-rich domain helps to mediate this UBQLN2-selective effect on tau.

Wild-type UBQLN2 appears to be intrinsically aggregate prone, and disease-related mutations may increase this aggregation propensity (Kim et al., 2018; Sharkey et al., 2018). Hence, the regulatory role of UBQLN2 in neurodegenerative disease may be complicated or compromised by its own aggregation propensity. Indeed, tau transgenic mice had elevated insoluble UBQLN2. Our observations in transgenic mice extended to human tauopathy disease brain tissue (PSP) in which high-molecular weight UBQLN2 was increased, underscoring the relationship between tau pathology and UBQLN2 disruption.

Based on our results in cells and mice showing that UBQLN2 lowered wild-type tau, we measured tau pathology and toxicity in genetic crosses of P301S mutant tau-expressing mice to mice overexpressing or lacking UBQLN2. Contrary to our expectation that an abundance of UBQLN2 would decrease mutant tau *in vivo*, UBQLN2 overexpression markedly increased phosphorylated tau and neurofibrillary tangle burden and precipitated premature hindlimb paralysis and death in mice. UBQLN2 knockout had the reverse effect, lowering the overall levels of tau in susceptible brain regions and decreasing phosphorylated tau pathology. These results support a model in which disruption in the balance in UBQLN2 impacts tau.

In our cell-based and mouse studies measuring endogenous tau, UBQLN2 effectively reduced nonaggregated tau. Thus, UBQLN2 may normally interact with soluble tau to regulate its levels. However, when tau is mutated, abnormally post-translationally modified or aggregated, UBQLN2 appears to lose the ability to regulate tau. It is possible that UBQLN2 enhances the targeting of tau to clearance pathways that are incompatible with handling tau in disease states. Alternatively, UBQLN2 may differentially interact with monomeric soluble tau and aggregated tau. Our immunoprecipitation results support the view that UBQLN2 physically interacts with tau, as previously shown for TDP-43 (Cassel and Reitz, 2013). The fact that tau species coprecipitating with UBQLN2 primarily run as monomer rather than as an aggregated or ubiquitinated smear suggests that UBQLN2 directly interacts with unaggregated tau. However, UBQLN2 rarely colocalizes with phosphorylated tau deposits in P301S mice. Our results in the P301S tauopathy mouse model combined with previous studies that failed to show UBQLN2 localization to tau in neurofibrillary tangles (Mori et al., 2012; Nölle et al., 2013; Rutherford et al., 2013) highlight a differential effect of UBQLN2 on healthy versus aggregated tau. Previous studies reporting that UBQLN2 does not interact with tau may have missed a narrow time window in which UBQLN2 can regulate tau before the system is overloaded with pathology. We suspect the mechanism by which UBQLN2 regulates tau likely differs from its regulation of other disease proteins such as Htt, with which UBQLN2 does interact in late-stage disease, specifically within disease protein aggregates (Mori et al., 2012; Zeng et al., 2015; Gerson et al., 2020). Our results also fail to detect a difference in Hsp70 in tau-expressing mice with and without UBQLN2, suggesting that the model (Hjerpe et al., 2016; Zhang et al., 2021), whereby Hsp70 facilitates UBQLN2 regulation of disease proteins such as Htt and dipeptide repeats in C9ORF72 FTD/ALS may not apply to tau.

Increasingly, the toxic synergy of various aggregate-prone proteins and their ability to "cross-seed" the misfolding/aggregation of native proteins have been implicated in the progression of mixed pathology disorders such as AD and PD (Guerrero-Muñoz et al., 2014; Sengupta et al., 2015). Hence, we evaluated whether UBQLN2-mediated exacerbation of tau pathology in P301S mice might simply be a by-product of its own aggregation. That appears not to be the case because overexpressing UBQLN2 even at low levels, where it remains diffuse and nonaggregated (Sharkey et al., 2020), also increased hyperphosphorylated tau and decreased survival. Moreover, UBQLN2 knockout had the opposite effect on tau pathology. Following up on our results in human disease tissue, we also evaluated whether tau pathology itself enhanced UBQLN2 puncta formation and aggregation. Tau pathology did not alter UBQLN2 puncta formation, further suggesting that the mechanism by which UBQLN2 and tau impact one another does not rely principally, if at all, on coaggregation of the two proteins.

Hyperphosphorylated tau in UBQLN2-overexpressing mice tended to accumulate in cells lacking UBQLN2 aggregates, favoring the hypothesis that under tauopathy disease conditions, UBQLN2 initiates changes to PQC pathways, thereby indirectly altering tau pathology. Supporting this idea, UBQLN2 overexpression and knockout led to changes in proteins involved in autophagy and ubiquitin-dependent protein clearance. However, a limitation of our study is that we do not yet understand how UBQLN2 affects tau pathology or know the factors driving phosphorylated tau pathology primarily in cells lacking robust UBQLN2 accumulation. Given that excitatory neurons which are selectively vulnerable to tau pathology also lack PQC regulators that modulate tau (Fu et al., 2019), it is possible that UBQLN2 primarily accumulates in cells that are more resilient to tau pathology. Alternatively, cells accumulating high levels of presumably aggregated UBQLN2 may in fact have little residual, functional UBQLN2, akin to UBQLN2 knock-out cells that display reduced phosphorylated tau. Neighboring cells accumulating phosphorylated tau may therefore contain higher than normal functional UBQLN2. UBQLN2 in these cells may initiate pathways that enhance the clearance of normal tau protein but fail to clear or potentially even stabilize aggregated tau. Thus, the failure of UBQLN2 to colocalize with NFTs in human disease

←

ubiquitin levels were markedly increased over all groups in UBQLN2-Hi crosses. LAMP2A and FKBP5 levels increased when UBQLN2 was overexpressed or knocked out, whereas levels of GSK3β increased and pGSK3β decreased as a function of elevated tau pathology. No significant differences were detected for p62, Hsp70, or Hsp90B. ***C***, To test whether increased ubiquitin levels reflect increased accumulation of ubiquitinated tau, tau protein was immunoprecipitated from whole-brain lysate of 9-month-old mice (characterized in Extended Data Fig. 5-1) and was analyzed for levels of ubiquitin. Ubiquitinated tau levels were unchanged in P301S mice with UBQLN2 overexpression. ***D***, P301SxUBQLN2-Hi transgenic mouse CA1 immunolabeled for p62, phosphorylated tau (AT8), and UBQLN2. ***E***, P301SxUBQLN2-Hi and P301SxUBQLN2 KO mice both have increased numbers of p62 puncta that localize to both tau and UBQLN2 ($n = 5–10$/group). ***F***, P301SxUBQLN2-Hi transgenic mouse CA1 immunolabeled for poly-ubiquitin (FK1), AT8, and UBQLN2 shows accumulation of ubiquitin localizing primarily to tau-negative cells. ***G***, P301SxUBQLN2-Hi transgenic mouse CA1 immunolabeled for LAMP2A, AT8, and UBQLN2. ***H***, P301SxUBQLN2-Hi mice have increased numbers of LAMP2A puncta that do not localize to tau aggregates ($n = 5–10$/group). Representative images for all groups are in Extended Data Figure 10-1.

(Mori et al., 2012; Nölle et al., 2013; Rutherford et al., 2013) or with phosphorylated tau inclusions in P301S mice may not tell the full story. As in work detailing a neighboring cell effect of poorly correlated dual pathologies in FTD, C9orf72, and TDP43 (Khosravi et al., 2020), the release of low levels of dysregulated UBQLN2 could impact tau clearance in neighboring cells. The propensity of both tau and UBQLN2 to phase separate may also imply a dynamic relationship that is altered when either tau and/or UBQLN2 forms stable aggregates (Zhang et al., 2017; Dao et al., 2018; Sharkey et al., 2018).

In summary, our results identify a role for UBQLN2 in modulating tau. Further study will be needed to understand what factors distinguish forms of tau that UBQLN2 can "handle" from those it cannot. While the mechanism by which UBQLN2 lowers wild-type tau protein levels and increases levels of aggregated and hyperphosphorylated mutant tau is still uncertain, our results point to PQC pathways of interest in mediating this effect. Changes to levels of autophagy proteins and ubiquitin, as well as the accumulation of ubiquitin and LAMP2A in cells lacking hyperphosphorylated tau, support a model by which UBQLN2 differentially initiates clearance or stabilization of tau depending on its conformational state. Previous studies have shown that whereas wild-type tau protein is largely degraded by CMA, mutations in tau and post-translational modifications inhibit CMA clearance of tau (Caballero et al., 2018, 2021). We hypothesize that UBQLN2 alters the balance of protein clearance pathways, activating CMA or potentially other pathways that accelerate clearance of wild-type, nonaggregated tau but trap and indirectly stabilize mutated or aggregated tau protein, preventing its degradation. Further understanding how UBQLN2 differentially regulates tau and other disease proteins may yield insights into the processes driving protein dyshomeostasis in tauopathies and other neurodegenerative diseases.

References

Andorfer C, Kress Y, Espinoza M, de Silva R, Tucker KL, Barde YA, Duff K, Davies P (2003) Hyperphosphorylation and aggregation of tau in mice expressing normal human tau isoforms. J Neurochem 86:582–590.

Archbold HC, Jackson KL, Arora A, Weskamp K, Tank EM, Li X, Miguez R, Dayton RD, Tamir S, Klein RL, Barmada SJ (2018) TDP43 nuclear export and neurodegeneration in models of amyotrophic lateral sclerosis and frontotemporal dementia. Sci Rep 8:4606.

Barmada SJ, Serio A, Arjun A, Bilican B, Daub A, Ando DM, Tsvetkov A, Pleiss M, Li X, Peisach D, Shaw C, Chandran S, Finkbeiner S (2014) Autophagy induction enhances TDP43 turnover and survival in neuronal ALS models. Nat Chem Biol 10:677–685.

Bertram L, Hiltunen M, Parkinson M, Ingelsson M, Lange C, Ramasamy K, Mullin K, Menon R, Sampson AJ, Hsiao MY, Elliott KJ, Velicelebi G, Moscarillo T, Hyman BT, Wagner SL, Becker KD, Blacker D, Tanzi RE (2005) Family-based association between Alzheimer's disease and variants in UBQLN1. N Engl J Med 352:884–894.

Brouwers N, Sleegers K, Engelborghs S, Bogaerts V, van Duijn CM, Paul De Deyn P, Van Broeckhoven C, Dermaut B (2006) The UBQLN1 polymorphism, UBQ-8i, at 9q22 is not associated with Alzheimer's disease with onset before 70 years. Neurosci Lett 392:72–74.

Burgess A, Vigneron S, Brioudes E, Labbé J-C, Lorca T, Castro A (2010) Loss of human Greatwall results in G2 arrest and multiple mitotic defects due to deregulation of the cyclin B-Cdc2/PP2A balance. Proc Natl Acad Sci U S A 107:12564–12569.

Caballero B, Wang Y, Diaz A, Tasset I, Juste YR, Stiller B, Mandelkow E-M, Mandelkow E, Cuervo AM (2018) Interplay of pathogenic forms of human tau with different autophagic pathways. Aging Cell 17:e12692.

Caballero B, Bourdenx M, Luengo E, Diaz A, Sohn PD, Chen X, Wang C, Juste YR, Wegmann S, Patel B, Young ZT, Kuo SY, Rodriguez-Navarro JA, Shao H, Lopez MG, Karch CM, Goate AM, Gestwicki JE, Hyman BT, Gan L, et al (2021) Acetylated tau inhibits chaperone-mediated autophagy and promotes tau pathology propagation in mice. Nat Commun 12:2238.

Cassel JA, Reitz AB (2013) Ubiquilin-2 (UBQLN2) binds with high affinity to the C-terminal region of TDP-43 and modulates TDP-43 levels in H4 cells: characterization of inhibition by nucleic acids and 4-aminoquinolines. Biochim Biophys Acta 1834:964–971.

Chuang K-H, Liang F, Higgins R, Wang Y (2016) Ubiquilin/Dsk2 promotes inclusion body formation and vacuole (lysosome)-mediated disposal of mutated huntingtin. Mol Biol Cell 27:2025–2036.

Cripps D, Thomas SN, Jeng Y, Yang F, Davies P, Yang AJ (2006) Alzheimer disease-specific conformation of hyperphosphorylated paired helical filament-tau is polyubiquitinated through Lys-48, Lys-11, and Lys-6 ubiquitin conjugation. J Biol Chem 281:10825–10838.

Dao TP, Kolaitis R-M, Kim HJ, O'Donovan K, Martyniak B, Colicino E, Hehnly H, Taylor JP, Castañeda CA (2018) Ubiquitin modulates liquid-liquid phase separation of UBQLN2 via disruption of multivalent interactions. Mol Cell 69:965–978.e6.

Deng H-X, Chen W, Hong S-T, Boycott KM, Gorrie GH, Siddique N, Yang Y, Fecto F, Shi Y, Zhai H, Jiang H, Hirano M, Rampersaud E, Jansen GH, Donkervoort S, Bigio EH, Brooks BR, Ajroud K, Sufit RL, Haines JL, et al (2011) Mutations in UBQLN2 cause dominant X-linked juvenile and adult onset ALS and ALS/dementia. Nature 477:211–215.

Doi H, Mitsui K, Kurosawa M, Machida Y, Kuroiwa Y, Nukina N (2004) Identification of ubiquitin-interacting proteins in purified polyglutamine aggregates. FEBS Lett 571:171–176.

Dumont M, Stack C, Elipenahli C, Jainuddin S, Gerges M, Starkova NN, Yang L, Starkov AA, Beal F (2011) Behavioral deficit, oxidative stress, and mitochondrial dysfunction precede tau pathology in P301S transgenic mice. FASEB J 25:4063–4072.

Edens BM, Yan J, Miller N, Deng H-X, Siddique T, Ma YC (2017) A novel ALS-associated variant in UBQLN4 regulates motor axon morphogenesis. eLife 6:e25453.

Elsasser S, Gali RR, Schwickart M, Larsen CN, Leggett DS, Müller B, Feng MT, Tübing F, Dittmar GAG, Finley D (2002) Proteasome subunit Rpn1 binds ubiquitin-like protein domains. Nat Cell Biol 4:725–730.

Fahed AC, McDonough B, Gouvion CM, Newell KL, Dure LS, Bebin M, Bick AG, Seidman JG, Harter DH, Seidman CE (2014) UBQLN2 mutation causing heterogeneous X-linked dominant neurodegeneration. Ann Neurol 75:793–798.

Flores BN, Li X, Malik AM, Martinez J, Beg AA, Barmada SJ (2019) An intramolecular salt bridge linking TDP43 RNA binding, protein stability, and TDP43-dependent neurodegeneration. Cell Rep 27:1133–1150.e8.

Fu H, Possenti A, Freer R, Nakano Y, Hernandez Villegas NC, Tang M, Cauhy PVM, Lassus BA, Chen S, Fowler SL, Figueroa HY, Huey ED, Johnson GVW, Vendruscolo M, Duff KE (2019) A tau homeostasis signature is linked with the cellular and regional vulnerability of excitatory neurons to tau pathology. Nat Neurosci 22:47–56.

Gerson JE, Safren N, Fischer S, Patel R, Crowley EV, Welday JP, Windle AK, Barmada S, Paulson HL, Sharkey LM (2020) Ubiquilin-2 differentially regulates polyglutamine disease proteins. Hum Mol Genet 29:2596–2610.

Gerson JE, Linton H, Xing J, Sutter AB, Kakos FS, Ryou J, Liggans N, Sharkey LM, Safren N, Paulson HL, Ivanova MI (2021) Shared and divergent phase separation and aggregation properties of brain-expressed ubiquilins. Sci Rep 11:287.

Guerrero-Muñoz MJ, Castillo-Carranza DL, Krishnamurthy S, Paulucci-Holthauzen AA, Sengupta U, Lasagna-Reeves CA, Ahmad Y, Jackson GR, Kayed R (2014) Amyloid-β oligomers as a template for secondary amyloidosis in Alzheimer's disease. Neurobiol Dis 71:14–23.

Hjerpe R, Bett JS, Keuss MJ, Solovyova A, McWilliams TG, Johnson C, Sahu I, Varghese J, Wood N, Wightman M, Osborne G, Bates GP, Glickman MH, Trost M, Knebel A, Marchesi F, Kurz T (2016) UBQLN2 mediates autophagy-independent protein aggregate clearance by the proteasome. Cell 166:935–949.

Jones CL, Njomen E, Sjögren B, Dexheimer TS, Tepe JJ (2017) Small molecule enhancement of 20S proteasome activity targets intrinsically disordered proteins. ACS Chem Biol 12:2240–2247.

Keller JN, Hanni KB, Markesbery WR (2000) Impaired proteasome function in Alzheimer's disease. J Neurochem 75:436–439.

Khosravi B, LaClair KD, Riemenschneider H, Zhou Q, Frottin F, Mareljic N, Czuppa M, Farny D, Hartmann H, Michaelsen M, Arzberger T, Hartl FU, Hipp MS, Edbauer D (2020) Cell-to-cell transmission of C9orf72 poly-(Gly-Ala) triggers key features of ALS/FTD. EMBO J 39:e102811.

Kim SH, Stiles SG, Feichtmeier JM, Ramesh N, Zhan L, Scalf MA, Smith LM, Pandey UB, Tibbetts RS (2018) Mutation-dependent aggregation and toxicity in a Drosophila model for UBQLN2-associated ALS. Hum Mol Genet 27:322–337.

Kuusisto E, Salminen A, Alafuzoff I (2002) Early accumulation of p62 in neurofibrillary tangles in Alzheimer's disease: possible role in tangle formation. Neuropathol Appl Neurobiol 28:228–237.

Malik AM, Miguez RA, Li X, Ho YS, Feldman EL, Barmada SJ (2018) Matrin 3-dependent neurotoxicity is modified by nucleic acid binding and nucleocytoplasmic localization. Elife 7:e35977.

Mizukami K, Abrahamson EE, Mi Z, Ishikawa M, Watanabe K, Kinoshita S, Asada T, Ikonomovic MD (2014) Immunohistochemical analysis of ubiquilin-1 in the human hippocampus: association with neurofibrillary tangle pathology. Neuropathology 34:11–18.

Mori F, Tanji K, Odagiri S, Toyoshima Y, Yoshida M, Ikeda T, Sasaki H, Kakita A, Takahashi H, Wakabayashi K (2012) Ubiquilin immunoreactivity in cytoplasmic and nuclear inclusions in synucleinopathies, polyglutamine diseases and intranuclear inclusion body disease. Acta Neuropathol 124:149–151.

Myeku N, Clelland CL, Emrani S, Kukushkin NV, Yu WH, Goldberg AL, Duff KE (2016) Tau-driven 26S proteasome impairment and cognitive dysfunction can be prevented early in disease by activating cAMP-PKA signaling. Nat Med 22:46–53.

Nölle A, van Haastert ES, Zwart R, Hoozemans JJM, Scheper W (2013) Ubiquilin 2 is not associated with tau pathology. PLoS One 8:e76598.

Rao H, Sastry A (2002) Recognition of specific ubiquitin conjugates is important for the proteolytic functions of the ubiquitin-associated domain proteins Dsk2 and Rad23. J Biol Chem 277:11691–11695.

Rutherford NJ, Lewis J, Clippinger AK, Thomas MA, Adamson J, Cruz PE, Cannon A, Xu G, Golde TE, Shaw G, Borchelt DR, Giasson BI (2013) Unbiased screen reveals ubiquilin-1 and -2 highly associated with Huntingtin inclusions. Brain res 1524:62–73.

Safren N, Chang L, Dziki KM, Monteiro MJ (2015) Signature changes in ubiquilin expression in the R6/2 mouse model of Huntington's disease. Brain Res 1597:37–46.

Safren N, Tank EM, Malik AM, Chua JP, Santoro N, Barmada SJ (2021) Development of a specific live-cell assay for native autophagic flux. J Biol Chem 297:101003.

Schaeffer V, Lavenir I, Ozcelik S, Tolnay M, Winkler DT, Goedert M (2012) Stimulation of autophagy reduces neurodegeneration in a mouse model of human tauopathy. Brain 135:2169–2177.

Scotter EL, Smyth L, JaWT B, Wong C-H, de Majo M, Vance CA, Synek BJ, Turner C, Pereira J, Charleston A, Waldvogel HJ, Curtis MA, Dragunow M, Shaw CE, Smith BN, Faull RLM (2017) C9ORF72 and UBQLN2 mutations are causes of amyotrophic lateral sclerosis in New Zealand: a genetic and pathologic study using banked human brain tissue. Neurobiol Aging 49:214.e1–214.e5.

Sengupta U, Guerrero-Muñoz MJ, Castillo-Carranza DL, Lasagna-Reeves CA, Gerson JE, Paulucci-Holthauzen AA, Krishnamurthy S, Farhed M, Jackson GR, Kayed R (2015) Pathological interface between oligomeric alpha-synuclein and tau in synucleinopathies. Biol Psychiatry 78:672–683.

Sharkey LM, Safren N, Pithadia AS, Gerson JE, Dulchavsky M, Fischer S, Patel R, Lantis G, Ashraf N, Kim JH, Meliki A, Minakawa EN, Barmada SJ, Ivanova MI, Paulson HL (2018) Mutant UBQLN2 promotes toxicity by modulating intrinsic self-assembly. Proc Natl Acad Sci U S A 115:E10495–E10504.

Sharkey LM, Sandoval-Pistorius SS, Moore SJ, Gerson JE, Komlo R, Fischer S, Negron-Rios KY, Crowley EV, Padron F, Patel R, Murphy GG, Paulson HL (2020) Modeling UBQLN2-mediated neurodegenerative disease in mice: shared and divergent properties of wild type and mutant UBQLN2 in phase separation, subcellular localization, altered proteostasis pathways, and selective cytotoxicity. Neurobiol Dis 143:105016.

Shimura H, Schwartz D, Gygi SP, Kosik KS (2004) CHIP-Hsc70 complex ubiquitinates phosphorylated tau and enhances cell survival. J Biol Chem 279:4869–4876.

Slifer MA, Martin ER, Bronson PG, Browning-Large C, Doraiswamy PM, Welsh-Bohmer KA, Gilbert JR, Haines JL, Pericak-Vance MA (2006) Lack of association between UBQLN1 and Alzheimer disease. Am J Med Genet B Neuropsychiatr Genet 141B:208–213.

Smemo S, Nowotny P, Hinrichs AL, Kauwe JSK, Cherny S, Erickson K, Myers AJ, Kaleem M, Marlowe L, Gibson AM, Hollingworth P, O'Donovan MC, Morris CM, Holmans P, Lovestone S, Morris JC, Thal L, Li Y, Grupe A, Hardy J, et al (2006) Ubiquilin 1 polymorphisms are not associated with late-onset Alzheimer's disease. Ann Neurol 59:21–26.

Stauffer W, Sheng H, Lim HN (2018) EzColocalization: an ImageJ plugin for visualizing and measuring colocalization in cells and organisms. Sci Rep 8:15764.

Weskamp K, Safren N, Miguez R, Barmada S (2019) Monitoring neuronal survival via longitudinal fluorescence microscopy. J Vis Exp (143):e59036.

Williams KL, Warraich ST, Yang S, Solski JA, Fernando R, Rouleau GA, Nicholson GA, Blair IP (2012) UBQLN2/ubiquilin 2 mutation and pathology in familial amyotrophic lateral sclerosis. Neurobiol Aging 33:2527.e3–2527.e10.

Wu H-PP, Ioffe JC, Iverson MM, Boon JM, Dyck RH (2013) Novel, whisker-dependent texture discrimination task for mice. Behav Brain Res 237:238–242.

Yoshiyama Y, Higuchi M, Zhang B, Huang S-M, Iwata N, Saido TC, Maeda J, Suhara T, Trojanowski JQ, Lee VMY (2007) Synapse loss and microglial activation precede tangles in a P301S tauopathy mouse model. Neuron 53:337–351.

Zeng L, Wang B, Merillat SA, Minakawa E, Perkins MD, Ramani B, Tallaksen-Greene SJ, do Carmo Costa M, Albin RL, Paulson HL (2015) Differential recruitment of UBQLN2 to nuclear inclusions in the polyglutamine diseases HD and SCA3. Neurobiol Dis 82:281–288.

Zhang K, Wang A, Zhong K, Qi S, Wei C, Shu X, Tu WY, Xu W, Xia C, Xiao Y, Chen A, Bai L, Zhang J, Luo B, Wang W, Shen C (2021) UBQLN2-HSP70 axis reduces poly-Gly-Ala aggregates and alleviates behavioral defects in the C9ORF72 animal model. Neuron 109:1949–1962.e6.

Zhang X, Lin Y, Eschmann NA, Zhou H, Rauch JN, Hernandez I, Guzman E, Kosik KS, Han S (2017) RNA stores tau reversibly in complex coacervates. PLoS Biol 15:e2002183.